

10
6/17/89 JS (1)

SANDIA REPORT

SAND88-3341 • UC-25
Unlimited Release
Printed April 1989

Did High-Altitude EMP Cause the Hawaiian Streetlight Incident?

Charles N. Vittitoe

Prepared by
Sandia National Laboratories
Albuquerque, New Mexico 87185 and Livermore, California 94550
for the United States Department of Energy
under Contract DE-AC04-76DP00789

**DO NOT MICROFILM
COVER**

MASTER

Issued by Sandia National Laboratories, operated for the United States Department of Energy by Sandia Corporation.

NOTICE: This report was prepared as an account of work sponsored by an agency of the United States Government. Neither the United States Government nor any agency thereof, nor any of their employees, nor any of their contractors, subcontractors, or their employees, makes any warranty, express or implied, or assumes any legal liability or responsibility for the accuracy, completeness, or usefulness of any information, apparatus, product or process disclosed, or represents that its use would not infringe privately owned rights. Reference herein to any specific commercial product, process, or service by trade name, trademark, manufacturer, or otherwise, does not necessarily constitute or imply its endorsement, recommendation, or favoring by the United States Government, any agency thereof or any of their contractors or subcontractors. The views and opinions expressed herein do not necessarily state or reflect those of the United States Government, any agency thereof or any of their contractors.

Printed in the United States of America. This report has been reproduced directly from the best available copy.

Available to DOE and DOE contractors from
Office of Scientific and Technical Information
PO Box 62
Oak Ridge, TN 37831

Prices available from (615) 576-8401, FTS 626-8401

Available to the public from
National Technical Information Service
US Department of Commerce
5285 Port Royal Rd
Springfield, VA 22161

NTIS price codes
Printed copy: A03
Microfiche copy: A01

DISCLAIMER

This report was prepared as an account of work sponsored by an agency of the United States Government. Neither the United States Government nor any agency Thereof, nor any of their employees, makes any warranty, express or implied, or assumes any legal liability or responsibility for the accuracy, completeness, or usefulness of any information, apparatus, product, or process disclosed, or represents that its use would not infringe privately owned rights. Reference herein to any specific commercial product, process, or service by trade name, trademark, manufacturer, or otherwise does not necessarily constitute or imply its endorsement, recommendation, or favoring by the United States Government or any agency thereof. The views and opinions of authors expressed herein do not necessarily state or reflect those of the United States Government or any agency thereof.

DISCLAIMER

Portions of this document may be illegible in electronic image products. Images are produced from the best available original document.

Did High-Altitude EMP Cause the Hawaiian Streetlight Incident?

Charles N. Vittitoe
Electromagnetic Applications Division
Sandia National Laboratories
Albuquerque, NM 87185

Abstract

Studies of electromagnetic pulse (EMP) effects on civilian and military systems predict results ranging from severe destruction to no damage. Convincing analyses that support either extreme are rare. The Hawaiian streetlight incident associated with the Starfish nuclear burst is the most widely quoted observed damage. We review the streetlight characteristics and estimate the coupling between the Starfish EMP and a particular streetlight circuit identified as one of the few that failed. Evidence indicates that the damage was EMP-generated. The main contributing factors were the azimuthal angle of the circuit relative to the direction of EMP propagation, and the rapid rise of the EMP signal. The azimuthal angle provided coherent buildup of voltage as the EMP swept across the transmission line. The rapid rise allowed substantial excitation before the canceling effects of ground reflections limited the signals. Resulting voltages were at the threshold for causing the observed fuse damage and are consistent with this damage occurring in only some of the strings in the systems.

MASTER

Acknowledgments

Clarence Mehl of Sandia National Laboratories (SNL) sparked my first interest in the Hawaiian streetlight incident. Since that input in the late 1960s, the intrigue has increased. The present work was prompted by recent availability of some of the missing streetlight data. Bernard R. Cooper, Physics Department at West Virginia University, organized a study on EMP sponsored by the American Physical Society (APS) Forum on Physics and Society and presided at their meeting that considered the EMP threat, presented to the APS in March 1985. As a result of part of this work, John Mattox of Stanford made a site visit to Hawaii, gathered as much data on the streetlight effect as possible, and presented results to the 1985 Forum meeting. His chief sources of information were F. William Souza, a foreman of the Honolulu City and County Street Lighting Department during 1962, and Alan S. Lloyd, Professional Engineer and Executive Staff Engineer at the Hawaiian Electric Company, Inc. During 1962 Lloyd was a sales engineer for the Honolulu Electrical Products Company, a Westinghouse distributor.

The description of the streetlight circuit is largely taken from Mattox's notes and from my telephone discussions with A. S. Lloyd and with F. W. Souza. Lloyd also found an isolation transformer of the type used in Figure 1. With the help of A. Jack Canute of SNL and Masao Bentosino, the present foreman of the Honolulu City-County Streetlight Department, the transformer was transferred to SNL for testing by N. I. Turner. Mario Rabinowitz of the Electric Power Research Institute brought my attention to notes from L. F. Wouters (later identified by data from W. C. Hart and W. A. Radasky, Metatech, as the Watson reports 00333/00334) that were formed soon after the Starfish burst. Rabinowitz also furnished data for typical surge impedances of isolation transformers. S. W. Holmes and George Seely, SNL, tested a series of streetlight cutouts to confirm that individual streetlight survival was to be expected.

John Malik, Los Alamos National Laboratory, is acknowledged for sharing many insights concerning EMP phenomena and for review of this report. The support of G. J. Scrivner and J. H. Renken at Sandia was vital. Helpful discussions with Scrivner and with K. C. Chen, R. D. Jones, J. D. Kotulski, D. A. Rieb, D. J. Riley, G. A. Seely, C. D. Turner, N. I. Turner, L. K. Warne, and W. Van Deusen of SNL are acknowledged. The report also benefited from technical reviews by R. L. Parker of Research and Development Associates, by J. Prewitt of Stanford Research Institute, International, by W. A. Radasky of Metatech, and by C. H. Eichler of Westinghouse Electric Corporation with his support by Randy Barnes of Oak Ridge National Laboratory. E. R. Voelker provided editorial skills. This work was funded by the US Department of Energy.

Contents

1. Introduction	7
2. Review of the Streetlight Circuit.....	9
2.1 Newspaper Accounts.....	9
2.2 Mattox Information.....	9
2.3 Wouters-Watson Information	11
2.4 Isolation Transformer Data	13
2.5 Photocell Hypothesis	14
3. Review of the EMP Threat: Starfish EMP at Oahu	15
4. Coupling Analysis	16
4.1 Source Terms for the Transmission-Line Equations	16
4.2 Line Voltage, Differential-Mode Excitation.....	16
4.3 Incident Polarization.....	18
4.4 Differential-Mode Voltage.....	18
4.5 Common-Mode Signals.....	20
4.6 Streetlight Survival	21
4.7 Additional Hardware Considerations	23
4.8 Energy Balance for Disk-Cutout Failure	24
5. Conclusions	26
References	27
APPENDIX A—Isolation-Transformer Impedance	29
APPENDIX B—Plane-Wave Excitation of a Two-Wire Transmission Line	31

Figures

1 Starfish-Honolulu burst geometry.....	8
2 Ferdinand Street series lighting system in 1962	9
3 Typical lighting network for loop driven by the isolation transformer	11
4 Typical pole arrangement for loops driven by the isolation transformer.....	12
5 The high-altitude EMP generated by Starfish, as seen at Honolulu.....	15
6 Incident-wave geometry for the transmission line.....	16
7 The angular factor $A(\psi, \phi)$ for transmission-line excitation by a vertically polarized incident wave.....	18
8 The angular factor $A(\psi, \phi)$ for transmission-line excitation by a horizontally polarized incident wave	18
9 Transmission-line connections at the isolation-transformer disk cutout	19
10 Incident EMP that provides a horizontal component of electric field that includes the reflected-pulse contribution.....	21
11 Real part of the streetlight-assembly impedance.....	22
12 Imaginary part of the streetlight-assembly impedance.....	22
13 Effective inductance of the streetlight assembly	22
14 View along Aleo, southeast, toward Ferdinand	23
15 View along Ferdinand toward the Aleo intersection and toward Johnston Atoll	24
16 A 2500-lumen streetlight of the type used in 1962.....	24

Tables

1 EMP quotes	7
2 Isolation-transformer cutout characteristics	10
3 Wouters-Watson data on repaired loops, repair date December 9, 1962	13
4 Estimate of cutout resistance after failure.....	25

Did High-Altitude EMP Cause the Hawaiian Streetlight Incident?

1. Introduction

Studies of the effects of EMP on civilian and military systems predict results ranging from severe destruction to no damage. At times this wide variation in predictions remains, even when confined to the same type of EMP interaction and to the same system. Table 1 lists some of the conflicting (and tongue-in-cheek) views. Actual (rather than simulated) EMP-interaction data do exist and should be analyzed. Examination of the data allows us to discard some of the conflicting studies. Examination can also verify that those features of the incident EMP which dominate the coupling are consistent with the observed effects.

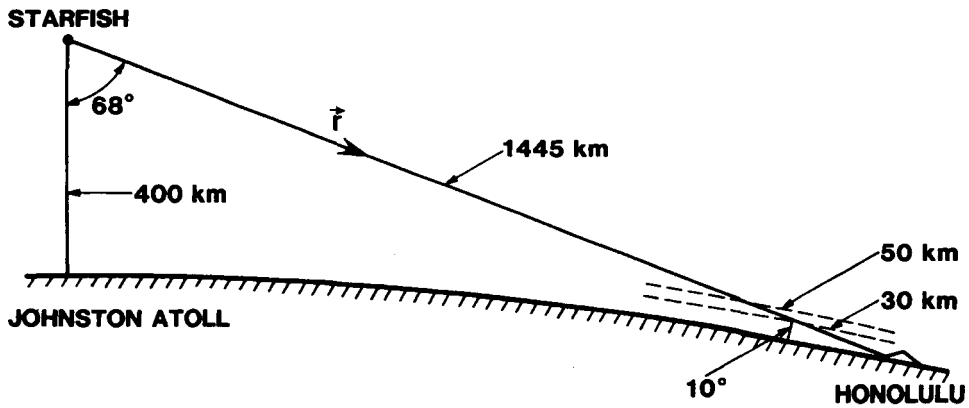
Table 1. EMP quotes (paraphrased)

EMP is not real (is <i>empty</i>)	—RAND
EMP is real, but who cares?	—USAF
EMP kills me	—Rich Wagner
EMP needs <i>empathy</i>	—Louis Wouters
EMP makes the world a completely ionized plasma	—Bill Broad
EMP <i>emphasizes employment</i>	—DNA
EMP suggests <i>empire</i>	—Bill Graham
EMP are the first three letters of “EMP is # \$ * % & ! @ #”	—C. P. “Skip” Knowles
EMP signifies photon rather than gluon exchange; an electromagnetic penguin	—High-energy theorist

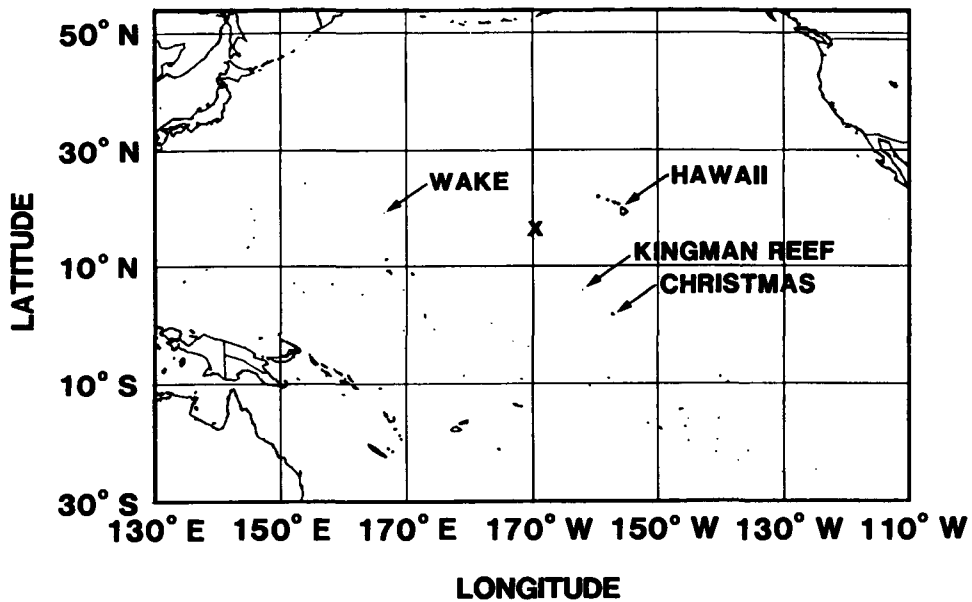
Several damage effects have been attributed to the high-altitude EMP. Tesche¹ notes the input-circuit troubles in radio receivers during the Starfish and Checkmate bursts; the triggering of surge arresters on an airplane with a trailing-wire antenna during Starfish, Checkmate, and Bluegill; and the Oahu

streetlight incident. The streetlight incident is repeatedly quoted in EMP reviews and seems to have originated with a report by S. Glasstone and P. J. Dolan,² who assert: “One of the best authenticated cases was the simultaneous failure of 30 strings (series-connected loops) of street lights at various locations on the Hawaiian island of Oahu, at a distance of 800 miles from ground zero.” The ground zero was for the Starfish burst at about 11 pm (Hawaiian time), July 8, 1962. The burst location was at 400 km over Johnston Atoll in the Pacific Ocean. With the attention surrounding the EMP threat over the last few years, one would expect that detailed analysis of available interaction data would be forthcoming; yet such details have been largely neglected. Even Glasstone and Dolan omit references or a basis for their assertion. M. Rabinowitz pointed out that even 30 strings of streetlights is a small percentage of the total number in the system and are not indicative of mass destruction of electrical systems.³ There have been suggestions⁴ that the 30 strings of streetlights is an overestimate of the EMP damage.

Here we examine the streetlight incident and test for consistency between the observed effects and those expected from limited analysis. If the EMP interaction with the lights was too small to have caused damage, the “best authenticated case” would be dismissed and the EMP would lose stature as a threat. If the EMP interaction was large, then all the lights would have been damaged. Since that did not occur, the EMP would again lose stature as a threat. Because of these rather narrow limits and the lack of many data points, because of the wide publicity attained, and because of the diversity in views concerning EMP, the streetlight incident is a crucial verification of the EMP threat to civilian systems. The geometry of the burst is shown in Figure 1.



BURST 30 km SW of J.A.
 AT 16° 28' N, 169° 38' W



HONOLULU 21.3° N, 157.6° W

JOHNSTON ATOLL 16.6° N, 169.3° W x

Figure 1. Starfish-Honolulu burst geometry

2. Review of the Streetlight Circuit

2.1 Newspaper Accounts (1962)

"The street lights on Ferdinand Street in Manoa and Kawainui Street in Kailua went out at the instant the bomb went off, according to several persons who called police last night," as reported on July 9, 1962, in the *Honolulu Advertiser*, a local paper. The article was reprinted in the Tuesday, February 21, 1984, edition that celebrated the 15th anniversary of Hawaiian statehood. The same article reports that the brilliant flash turned Hawaii's night into day, with the "spectacular pyrotechnic aftermath" lasting for 7 minutes. "It was like turning on all the lights all over the Hawaiian Islands for a super-super athletic contest."

The Saturday, July 28, 1962, edition of the *Honolulu Star-Bulletin* included an article by Robert Scott (of their staff and also a professor at the University of Hawaii) that reviewed "What Happened on the Night of July 8?" He reported that a City-County streetlight department official in Honolulu attributed blown circuit fuses in nine areas to energy from the bomb.

In the April 8, 1967, issue of the *Star-Bulletin*, Cornelius Downes described the fuses that failed, causing about 300 City streetlights to go out. They were "small black plastic rings with two disks of lead separated by thin, clear-plastic washers." The fuses were slightly smaller than a quarter. The article indicated that about two-thirds of Oahu's lighting system used such fuses.

2.2 Mattox Information*

John Mattox⁵ provided the data for Figure 2 on one streetlight loop that suffered damage: the Ferdinand Street loop in Manoa. His information was based on field work in Hawaii, on discussions with streetlighting personnel, and on the newspaper accounts. Some 30 strings of streetlights failed, about 1% of the lights existing at the time. The failure of 30 strings was well beyond any expectations for severe storms (where ~4 failures were typical). He concludes that the failures are definitely associated with the Starfish explosion.

*1984, with updates from A. S. Lloyd, F. W. Souza, and M. Bentosino

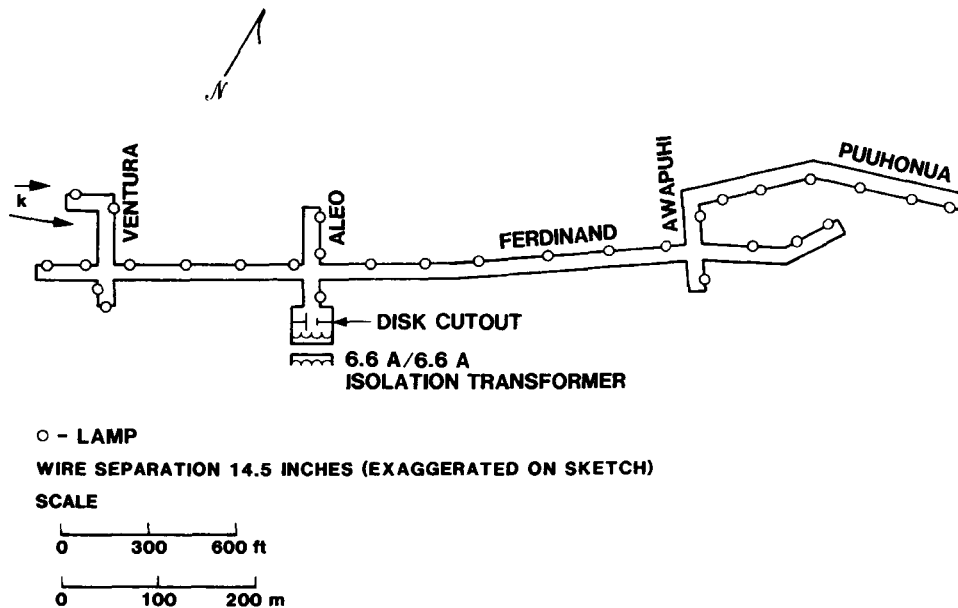


Figure 2. Ferdinand Street series lighting system in 1962

The lighting circuits were 6.6-A series circuits, with each incandescent bulb protected by a small disk cutout (fuse) in parallel with the base of each lamp. The small disk cutout provided continuity when a filament failed. Typically, 50 to 90 V across the filament leads caused a spark that created a shunt path through the cutout. These cutouts were about the size of a dime. When such failures occurred, the circuits were repaired by replacing the filament (the bulb) and the disk cutout. However, none of these small disk cutouts for individual streetlights were responsible for the failures recorded. Larger disk cutouts in another part of the circuit were responsible for the streetlights going out.

In some areas the available wire locations on the lighting poles required a reduced voltage from the high values needed for the long series circuits. An isolation transformer at a lower voltage then supplied current for these small loops of about 20 streetlights. The secondary winding of the isolation transformer was also shunted by a disk cutout (of a size intermediate between a nickel and a quarter and described in the newspaper accounts). If the isolated loop is broken, then the high voltage created in the open circuit would cause the disk cutout to arc, allowing the 6.6 A to flow through the disk cutout. When such failures occurred, the circuits were repaired by filing the shunt path on the Pb disks and reinserting the disks with their insulating washers. At times the cutout would fail at replacement. Then the filing might be repeated and an additional washer added. In all the circuits that failed on July 8, 1962, the failures were in the disk cutouts across the secondary in isolation transformers. No filaments or other components of the lighting system were damaged.

It was not possible to identify the particular lighting circuits that failed back in 1962. Official records were kept for 10 years or less. The series streetlighting systems have been replaced largely by lamps that are each controlled by a separate photocell. The new sodium vapor lamps are driven by 120 V from power-utility secondary lines. In 1962 the streetlights were owned and operated by the City and County of Honolulu, not by the power company, Hawaiian Electric.

Mattox found drawings of part of the series lighting system, retained by the City of Honolulu and reproduced as Figure 2. The circuit was basically a 3000-ft-long (914 m) horizontal loop that was 14.5 in. (36.8 cm) wide. The loop was not grounded and was activated by a 6.6-A isolation transformer. Wiring details are ambiguous at intersections such as where Puuhonua and Ferdinand come together in Figure 2. The wire with the streetlights on Ferdinand Street

may have been connected to the wire with streetlights on Puuhonua Street, or it may have been connected to the wire that continued down Ferdinand Street.

The isolating transformers came in several sizes. Alan S. Lloyd of the Hawaiian Electric Company, Inc. recalls that the options were as listed in Table 2, with the number of streetlights on each isolated circuit determining the required size.

Table 2. Isolation-transformer cutout characteristics

Transformer Rating (kVA)	Disk Cutout Burnthrough Voltage (V)
4	750 to 1200
5	1000 to 1200
7.5	1500 to 2100
10	2000 to 3000

In 1988, C. N. Vittitoe obtained samples of this type of disk cutout from Masao Bentosino of the Streetlight Department. The samples had the General Electric Catalog Number 3986079G7 and were for a 7.5-kVA or a 10-kVA system. The average breakdown voltage was listed as 2700 V. The breakdown-voltage difference from Table 2 is not understood. It likely results from a change in cutout design. The cutouts were roughly as described in the newspaper accounts. The thin clear-plastic insulators had a diameter of 14 mm with a 6.4-mm-dia hole in their center. The arcs occurred across the air gap in the center of the disks, not across the insulators. The ~40-mil (1-mm) gap thickness estimated as appropriate for the cutouts used in the 5-kVA transformers suggests the breakdown field strength of 10^6 V/m, near that expected for sea-level air. Moisture and temperature variations as well as Pb-surface-roughness differences may account for a portion of the variation in burnthrough voltage in Table 2. The listed values are handbook values. It is likely that the spread in burnthrough voltage is wider after several repair operations. The breakdown voltages could possibly be limited to 60-Hz signals, or they could also be appropriate for lightning-induced transients. As discussed later, at failure after the arc forms in the cutout, the isolation transformer provided the energy required to melt a portion of the Pb disk and form the permanent short across the cutout.

Samples of the type of disk cutouts used in the individual streetlights were also obtained. These cutouts for series sockets had General Electric Catalog Numbers 4815920-G1 and 4815920-G3 with breakdown voltage labeled Medium (100 to 200 V) and

High (250 to 350 V). The G1 cutouts were used with 4000- and 6000-lumen lamps. Those labeled G3 were for 10000-lumen lamps. The 50 – 90 V breakdowns came from a similar type of cutout that was used with the more prevalent 2500-lumen lamps. Westinghouse produced cutouts with a different design. The choice of brand usually varied with the sale price when the need arose.

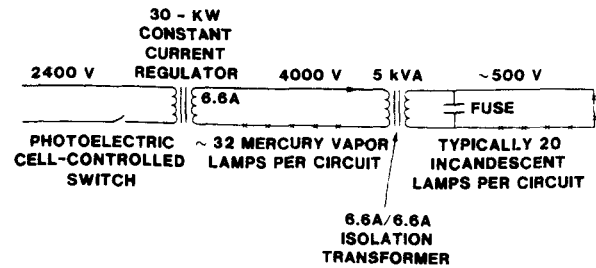
2.3 Wouters-Watson Information*

L. F. Wouters of Lawrence Livermore National Laboratory (LLNL) has made many contributions to the understanding of EMP phenomenology and interactions. One of his earliest contributions was recognition of the importance of collecting data on electrical damage associated with the Starfish explosion. About 1963, his group at LLNL sent Jim Watson to Honolulu to gather information on the streetlight damage. Some of Watson's notes are the basis for these data.⁶ The main sources of information are recorded as William Peterson, Samuel Ii, and Francis William (Willy) Souza (the lineman foreman), all of the City and County of Honolulu, which was the organization responsible for repairing the damaged circuits. Willy Souza is the same foreman who was acknowledged as a source for John Mattox.

The data indicate that about 30 strings of streetlights went out on Oahu and most of the circuits were in Honolulu. Records (no longer available during the Mattox search) show repair work on July 9, 1962. Watson gives a diagram (Figure 3) of a typical lighting network of the type that exhibited trouble. His data indicate that the 5-kVA entry in Table 2 is the proper choice.

In Figure 3, the utility-company line furnishes power to the constant-current regulator by means of a photoelectric-cell-controlled switch. The 2400 V at the regulator is provided by a phase-to-neutral connection on the incoming 4160-V (phase-to-phase), 3-phase, 4-wire, wye-connected utility power. The electric power community refers to this incoming line as a 4-kV line. However, we will call this incoming line a "2400-V" line and reserve "4000 V" to refer to the line so labeled in Figure 3.

*~1963, with updates from A. S. Lloyd, F. W. Souza, and M. Bentosino



FUSE IS SOURCE OF DIFFICULTY, STARFISH - ASSOCIATED, JULY 8, 1962
23 REPORTED REPLACEMENTS ON JULY 9, 1962
0 NORMAL

Figure 3. Typical lighting network for loop driven by the isolation transformer

The 30-kW regulator in Figure 3 with the 6.6 A it provided indicates that the power source for the labeled 4000-V line could furnish up to 4.5 kV. The utility distribution equipment that provided power to the 2400-V line had a 60-kV BIL rating (basic impulse insulation level, a measure of lightning protection) and suffered no damage. It is likely that the current regulator with its 6.6-A secondary driving the 4000-V series line also had a 60-kV BIL rating. The 4000-V and 500-V labels should not be considered as fixed values. The current regulator was often set at 6.5 A rather than 6.6 A to prolong lamp life. Once set, the current was regulated and fixed (except for transients caused by electromagnetic interference). The voltages varied somewhat, depending on the number of streetlights in the circuit.

The secondary, 500-V #6-gage medium-hard-drawn copper line typically held ~20 lamps, to furnish 25 V per lamp.⁷ Circles in Figure 2 represent 30 lamps. Thus, this circuit was a 750-V line, the maximum voltage allowed at the pole position where the secondary loops were mounted. Figure 2 shows a 2-wire system where the return wires are located on the same poles as the lights. About 80% of Honolulu used such a system. The rest used a single-wire system, where much more area was enclosed within the loop. No preference was obvious for damage to occur on either type of system.

Wouters' notes indicate that the wiring scheme was unusual. The electric utility had converted many of their distribution circuits (2400 V phase to neutral

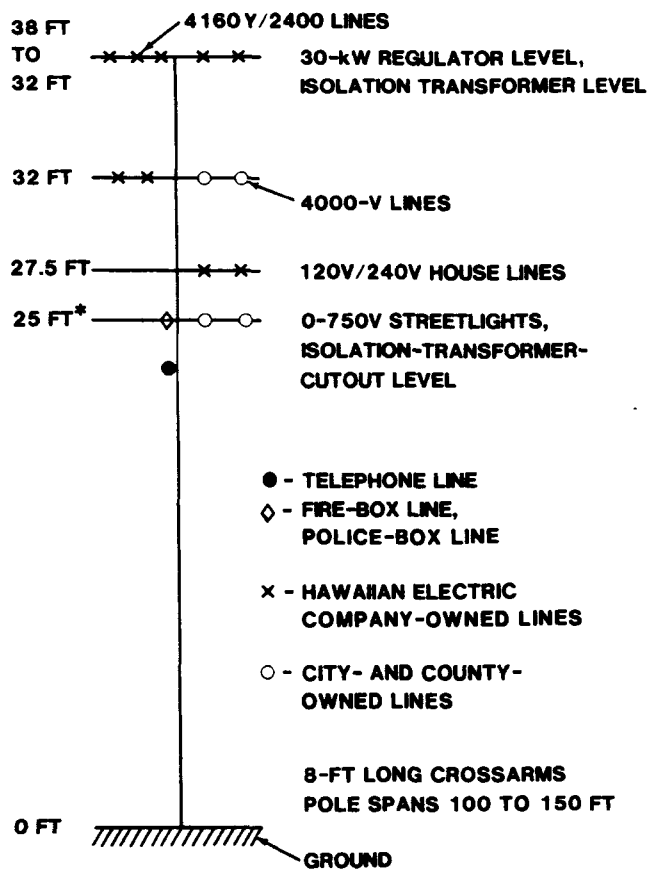
in Figure 3) to 12 kV (7200 V phase to neutral) to meet increased power demands. However, the City and County of Honolulu was gradually phasing out its 6.6-A series systems and did not want to purchase new 30-kW constant-current regulators with 7200-V primaries. The utility provided 7200-V to 2400-V step-down transformers so that the existing 30-kW regulators could remain in service until the 6.6-A series systems were eliminated. Few had been eliminated by July 1962.

Figure 4 shows a typical pole arrangement. The 4000-V and 500-V lines have been owned and operated by the City and County of Honolulu. One string of lights is described as perhaps covering a linear distance of ~5 city blocks, but at times circling blocks or meandering back and forth.

The 4000-V lines typically had ~28 mercury vapor lamps plus perhaps two isolation transformers driving the incandescent-lamp secondary circuits of the type that failed. Each 400-W mercury vapor lamp required ~1-kW driving capacity to provide the needed starting surge. The secondary isolated circuits were used at side streets characteristic of residential neighborhoods where short poles left no room for the 4000-V lighting systems. The only place where the 4000-V and 500-V lines had the arrangement in Figure 4 is where the isolation transformer made the transition from the primary to the secondary lamp circuit. The 500-V line proceeded from this origin to a series of shorter poles. Alan Lloyd indicated that the uppermost lines were reserved by Hawaiian Electric. The City-County lines at 4000 V and 500 V were at smaller heights, as indicated in Figure 4.

Twenty-three strings are recorded as having been repaired after Starfish (Table 3). The actual number of failures may be higher than 23 for two reasons noted by Wouters and Watson: (1) the records that were scanned did not cover all the districts, and (2) the records are likely to be incomplete. The repairman expected to replace the disk cutout and then

search for a break in the loop. Such breaks were not present on July 9, 1962. The damaged cutout was repaired in ~5 min. Several hours were typical to repair broken lines. Since the 5 min completed the repair, it is likely that some were not recorded. Recent discussion with Willy Souza indicates that many more than the 23 listed strings were damaged. Workmen took short cuts on paperwork on July 9, 1962, because of the number of failures and the large area where failures occurred.



*STREETLIGHT LINES WERE AT 27 FT ON SOME POLES

Figure 4. Typical pole arrangement for loops driven by the isolation transformer

Table 3. Wouters-Watson data on repaired loops, repair date December 9, 1962

Area	Street	Terrain	Street (s) or Wiring (w)* Angle from True North (°)
Manoa	Woodlawn	Deep Valley	53 (s)
Manoa	Ferdinand	Mountainside	56 (w&s)
Manoa	Lowrey	Deep Valley	36 (s)
Manoa	Round Top Drive	Face of Mountain	—
Near Manoa	Makiki Hts	Face of Mountain	19 (s)
Honolulu	Birch	Flatland	22 (s)
Honolulu	Algaroba	Flatland	70 (s)
Near Waikiki	Date	Flatland	71 (s)
Near Waikiki	Coral	Flatland	49 (s)
Kaimuki	Campbell Ave	Flatland	16 (s)
Kaimuki	Kealakula	Flatland	—
Kaimuki	Kanaina & George	Flatland	74 (s)
Kahala	Black Point Rd	Coastline	42 (s)
Near Manoa	Kaiki (6)	Flatland	—
Leeward District (4)		Flatland	—

*No entry occurs for streets where orientation could not be determined. The wiring orientation does not necessarily follow the street orientation.

In Table 3 the column for orientation angle has been added to the LLNL data to test for a possible strong correlation with the damage. Such a correlation is not apparent. Perhaps knowledge of wiring orientations would show better correlation. Angles at $\sim 66^\circ$ correspond to alignment with a horizontal projection of the line of sight to the burst. Figure 3 suggests that a cross street might orient some wiring at 90° to the listed street, giving an equivalent avenue of excitation near 24° from north. Seven of the 11 angles in Table 3 are within 10° of these two angles, 66° and 24° . With a random distribution, we would expect about five.

Table 3 is consistent with the newspaper account for Ferdinand Street. The table is also consistent with Robert Scott's finding of blown fuses in nine areas of Honolulu. However, the Kawainui-Street incident (mentioned in newspaper accounts and at 49° s orientation) in the Kailua Area does not appear in the table. This location is on the opposite side of the Koolau Mountain Range, away from Johnston Atoll. Perhaps this district was not scanned by the Watson search. (Kealakula Street does not appear on the maps at hand; this entry may have been Kealaolu as noted in one newspaper account.)

2.4 Isolation Transformer Data

Isolation transformers with the 5-kVA rating were bolted directly to the pole at ~ 38 ft (11.6 m) from the ground. (More than 750 V was not allowed at the ~ 25 ft level.) Connections from the transformer to the disk cutout in Figure 2 were by #8-gage wires, with 5000-V insulation. The two wires were enclosed within a ~ 1 -in.- dia plastic pipe mounted along the pole and under the crossarm to where the streetlight wires were located. The disk cutout was at the 25-ft level, on the streetlight crossarm.

Handbook data are available for typical pole-mounted, single-phase, 60-Hz distribution transformers rated at 5 kVA.⁸ Unfortunately, the handbooks examined give no data for the constant-current isolation transformers. The 1962 circuit in Figure 3 requires capability for ~ 750 V on the secondary, and so the rating on the primary winding must be >750 V (assuming a little power loss in the transformer). Information from Stig Nilsson at the Electric Power Research Institute (EPRI) indicates that the transformer impedance at high frequencies is often dominated by capacitive reactance (from bushing, interwinding, and possible shield capacitance within

the transformer). At high frequencies, large transformers were indicated to have a typical capacitance near 2 nF. An early estimate of the coupling used this value to find the isolation-transformer surge impedance.⁹ During that early analysis it was assumed that the isolation transformer was mounted close to its protective disk cutout. This was an option since the transformers had contacts available. However, these contacts were kept open (typically by inserting a portion of a popsicle stick), allowing the disk cutouts to be mounted ~13 feet below the transformer, at the 25-ft level. At this lower position, cutouts could be replaced more easily, and less-threatening voltages were nearby during the replacements.

Masao Bentosino, present foreman at the Streetlight Department, provided a constant-current isolation transformer that was stored in their warehouse (although no longer used). This transformer has a 2-kVA rating at 6.6 A and is sufficient to service a 12-streetlight system. Measurements of the secondary impedance are given in Appendix A.

2.5 Photocell Hypothesis (~ 1962)

The dramatic lighting of the night sky over Hawaii suggested to Don Shuster of Sandia National Laboratories that the streetlight effects could have been caused by photocells reacting to the pyrotechnic display.¹⁰ The light would automatically turn the streetlights off, then on. At a typical sunset (sunrise) the streetlights come on (off) in a staggered manner dependent on the slow setting (rising) of the sun, on the sensitivity of the photodiode, and on the presence of shadows. The light on the night of July 8, 1962, was turned off and on much faster than at a typical sunrise and sunset; the synchronized demand to alter many lights at once might have stressed the system and created the failures. A rapid rate of change of current in the 4000-V line, for example, could overstress the 500-V line and allow either onset or extinction of the light to cause the experienced damage.

Information from A. S. Lloyd and W. F. Souza indicates that the 30-kW current regulators were switched on by a photoelectric cell. The oil switch directed the 2400 V into the 30-kW regulator and then into the 4000-V line. In Figure 3 the switch was added to the Watson data to represent action of the photoelectric cell.

Discussion with Ralph Partridge (Head of the Electrical Engineering Department at the University of Hawaii during 1962, presently at Los Alamos National Laboratory) indicated that such photocells had built-in delays before switching occurred. The delays required that the change in illumination remain for several seconds to several minutes. This prevented fast response to a sudden light, eliminating switching caused by temporary exposure to headlights, spotlights, searchlights, lightning flashes, or to cloud or airplane shadows as they cross the sun. Such delays make synchronized switching unlikely.

The inductance for the 4000-V line is estimated at 20 mH plus the inductance in the isolation transformer and in the 30-kW current regulator. At 60 Hz the impedance of the line was ~600 Ω , dominated by resistance in the lamps. The peak dI/dt is estimated as the voltage applied by the current regulator divided by the inductance. Any increase in dI/dt because of synchronization of many photocells might increase this voltage. However, it appears that this could happen only by sending the power generator into a transient that should be damped by protective equipment. Power companies go to extremes to try and eliminate high-frequency transients to improve line regulation at 60 Hz. The 30-kW power rating of the constant current regulator is a small fraction of the load on the power generator. Load changes that are associated with Super-Bowl halftimes or other special events or associated with sudden weather changes are much more stressing to the power generators and to the system stability. The applied voltage is expected to remain bound by the 4000 V in Figure 3, which limits the dI/dt to values near those experienced when sunlight drives the photocells. Thus the photocell hypothesis is discarded.

Further support for rejection of the photocell hypothesis comes from an eyewitness account. When Starfish occurred, A. S. Lloyd was standing on a residential hillside a mile east of Pearl Harbor, Oahu. No streetlight extinctions were noticed within his field of view. The light over Johnston Atoll did not cause widespread photocell switching. As the darkness returned and extinguished lights would come back on, the incandescent lights would come on with the photoswitch and the mercury-vapor streetlights would delay 5- to 10-minutes before turning on. No such switching was noticed by this witness or was recorded in news accounts. Perhaps the usual practice of aiming photocells directly overhead or toward the northern sky helped prevent such switching.

3. Review of the EMP Threat: Starfish EMP at Oahu

Estimates are available for the early-time high-altitude EMP created by the Starfish burst and arriving at Honolulu.¹¹ The dip angle of the geomagnetic field in the gamma-ray absorption region was taken as 35°, with the observation point at 54.3° east of the magnetic north direction. Figure 5 shows the transverse EMP generated by the 1.4 kT of gamma rays (used in the calculations¹¹). The peak amplitude at Honolulu is 5.6 kV/m, with a 10% to 90% rise time of ~38 ns. As pointed out,¹¹ the pulse is not saturated and does not represent a worst-case pulse. Higher weapon yields and increased geomagnetic fields in the gamma-ray absorption region of the atmosphere (as would be experienced over the central US, for example) would result in larger peak EMP fields. Although Reference 11 does not provide an uncertainty for this incident EMP, simplifications in the Starfish output used in the calculation and in the EMP codes are judged to give accuracy within a factor of 2.

Aside from the early precursor, the rise to peak can be approximated by $5600 \text{ V/m} \sin[26.624 t(\mu\text{s})]$. This representation requires 59 ns to reach the peak and has the 38-ns rise time. The fall requires lower frequencies.

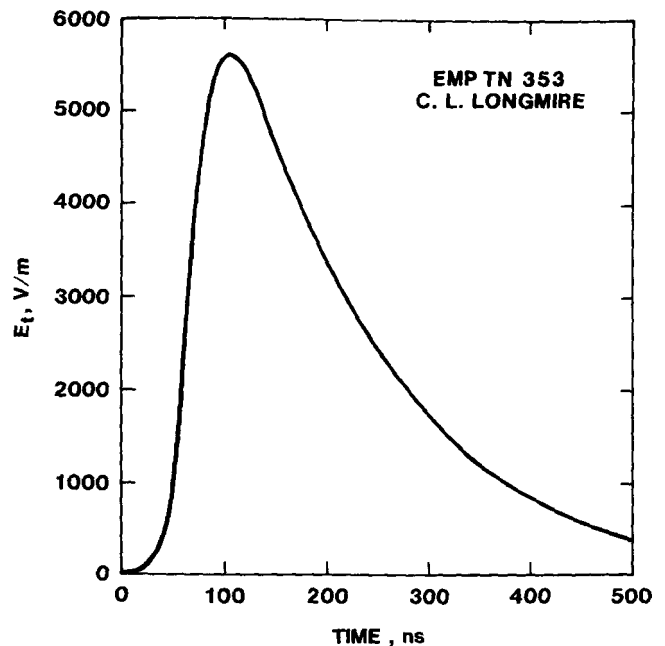


Figure 5. The high-altitude EMP generated by Starfish, as seen at Honolulu

4. Coupling Analysis

4.1 Source Terms for the Transmission-Line Equations

The lighting circuit is roughly modeled as a two-wire, straight transmission line of length p , with terminating impedances Z_1 and Z_2 at the two ends. The transmission line equations are developed in Appendix B. The incident EMP is treated as a plane wave, locally incident at Ferdinand Street and illustrated by the propagation vector \mathbf{k} in Figure 6.

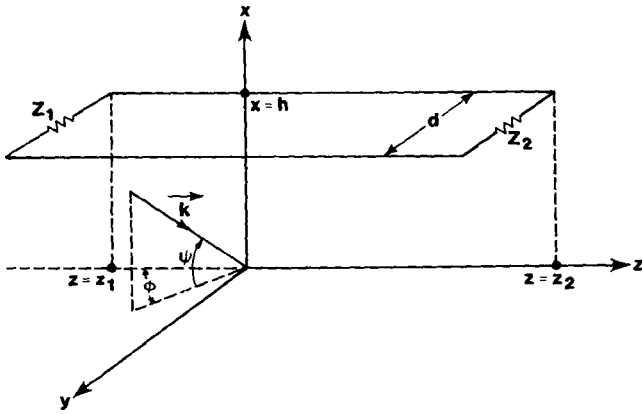


Figure 6. Incident-wave geometry for the transmission line

With incident amplitude E_i and with phase given by $\exp(i\mathbf{k} \cdot \mathbf{x})$, the incident field at the wire is given by

$$E_i e^{i\mathbf{k} \cdot \mathbf{x}} = E_i \exp[ikz \cos \psi \cos \phi - ik(x-h) \sin \psi -iky \cos \psi \sin \phi] . \quad (1)$$

The $e^{-i\omega t}$ time dependence is understood. The phase is defined to be zero at $x = h$, $y = 0$, and $z = 0$, where the coordinate system is given in Figure 6. The incoming wave is propagating along \mathbf{k} (the direction of the Poynting vector) with elevation angle ψ and with the azimuthal angle ϕ shown in the $y - z$ ground plane. One wire is parallel to the z axis at $x = h$, $y = 0$. The second wire in the line is at the same height, h , but displaced to a position with $y = d$, as Figure 6 shows.

The incident electric field is orthogonal to \mathbf{k} . It is convenient to separate two cases of linear polarization for the incident wave-horizontal polarization where \mathbf{E} is parallel to the $y - z$ plane, and vertical polarization where the incident \mathbf{E} is in the $\mathbf{k} - x$ plane. This convenience aids breaking the field into x , y , z components and allows for changes in the ground-reflection coefficients. At high ground conductivity, the vertical polarization gives a reflection coefficient $R_V = +1$ and horizontal polarization gives $R_H = -1$ for this idealized case.¹²

The wave reflected from the ground arrives at the wire with a time delay $t_o = 2h \sin \psi/c$ relative to the direct wave. The vertically polarized wave then gives an electric field at the wire given by

$$E_x(h,z) = E_i e^{i\mathbf{k} \cdot \mathbf{x}} (1 + R_V e^{i\omega 2h \sin \psi/c}) \cos \psi , \quad (2)$$

$$E_y(h,z) = -E_i e^{i\mathbf{k} \cdot \mathbf{x}} (1 - R_V e^{i\omega 2h \sin \psi/c}) \sin \psi \sin \phi , \quad (3)$$

$$E_z(h,z) = E_i e^{i\mathbf{k} \cdot \mathbf{x}} (1 - R_V e^{i\omega 2h \sin \psi/c}) \sin \psi \cos \phi . \quad (4)$$

The corresponding components for horizontal polarization are:

$$E_x(h,z) = 0 , \quad (5)$$

$$E_y(h,z) = -E_i e^{i\mathbf{k} \cdot \mathbf{x}} (1 + R_H e^{i\omega 2h \sin \psi/c}) \cos \phi , \quad (6)$$

$$E_z(h,z) = -E_i e^{i\mathbf{k} \cdot \mathbf{x}} (1 + R_H e^{i\omega 2h \sin \psi/c}) \sin \phi . \quad (7)$$

In our simplified analysis we use reflection coefficients appropriate for a high-conductivity ground. Because we are examining voltage differences between two wires above a ground plane, use of realistic ground conductivities is expected to make little difference.

4.2 Line Voltage, Differential-Mode Excitation

Figure 2 shows the circuit for the Ferdinand lighting system. Many problem parameters remain a mystery: surge impedance of the actual isolation transformer, reflection coefficients at each line discontinuity and at the ground, efficiencies for converting common-mode current on the 4000-V line into

differential excitation of the 500-V line, geometry for the 4000-V line, geometry for nearby structures and their scattering effects on the incoming wave, ... Detailed calculations are not justified because of such uncertainties.

The differential current, I , and differential voltage, V , developed in Appendix B are the circuit current and voltage in the transmission line that are excited by the incident EMP. These excitations are superimposed on the current and voltage normally in the lines (expected to be ~ 6.6 A and ~ 750 V), driven by the isolation transformer. The 60-Hz line has a long oscillation period ($1/f = 16.7$ ms) as compared with the pulse width in Figure 5 (full width at half max = 165 ns). The superposition was a spike in the sinusoidal signal. The lines in Honolulu are likely driven in phase; at 60 Hz the wavelength is 5000 km. Whether or not the spike occurs with a phase that adds constructively depends on the instantaneous line phase and on orientation effects that determine the sign of the induced voltage.

Of all the streetlights that were exposed, only the fraction that were in the short-pole residential areas where reduced voltage was required would have the type of secondary circuit that was damaged. Only a rough value is available for this fraction; $\sim 67\%$, estimated by the *Honolulu Star-Bulletin* in a 1967 newspaper account. To sustain damage we might also speculate that the line voltage must be set for 750 V. If that (unknown) portion of secondary isolated circuits being driven at 750 V were 10% of the total number of secondary isolated circuits, the 30 failed strings suggests that 15% rather than 1% of the *susceptible* circuits failed. Only more data about the old lighting system and the particular circuits that failed can justify such an estimate and speculation.

As described in Appendix B, we assume an $e^{-i\omega t}$ time dependence and find the line voltage to be $V(z) = V_y^{(s)}(z) + Z_o([K_1 + P(z)] e^{ikz} - [K_2 + Q(z)] e^{-ikz})$. The notation is described in Appendix B. Figure 2 suggests that the differential-mode end impedance $Z_1 = 0$ is appropriate. To obtain an (upper bound) estimate for the voltage at position 2, we take $Z_2 = \infty$. We also fix the origin of our z axis by choosing $z_1 = -p$, $z_2 = 0$.

Evaluating $V(z)$ at $z = 0$ gives $V(0) = V_y^{(s)}(0) + Z_o[K_1 - K_2 + P(0)]$. Results from Appendix B allow this open-circuit voltage, V_{oc} , to be written as

$$V(0) = -E_y^{inc}(h,0,0) d + 2Z_o P(0) + \frac{E_y^{inc}(h,0,-p) d}{\cos kp} + \frac{Z_o e^{ikp}}{\cos kp} [Q(-p) - P(0)]. \quad (8)$$

The phase factor e^{ikp} introduces a time delay of p/c . At the beginning of the interaction when the leading edge of E_i just reaches $z_2 = 0$, only the first two terms can affect the solution at $z = 0$. If the wave reaches z_1 at $t = t_1$ and reaches z_2 at $t = t_2$, then for the interval $t_2 \leq t \leq t_1 + p/c$ the terms with the e^{ikp} factor cannot contribute to the open circuit voltage at $z_2 = 0$. The second $P(0)$ term contributed by $K_1 - K_2$ represents the voltage-doubling effect produced by reflection from an open circuit. (A matched load at $z = z_2$, instead of an open circuit, will discard the factor 2 and indicate the variation expected because of the unknown surge impedance of the isolation transformer.) The $E_y^{inc}(h,0,-p)$ term also requires a time $t_1 + p/c$ to begin affecting the signal at $z = 0$. Within the restricted time interval ($t_2 \leq t \leq t_1 + p/c$) the voltage becomes $V(0) = -E_y^{inc}(h,0,0) d + 2Z_o P(0)$, or

$$V(0) = -E_y^{inc}(h,0,0) d + \frac{A_1(\psi,\phi) d E^{inc}(h,0,0)}{1 - \cos \psi \cos \phi} \times [1 - e^{ikp(1 - \cos \psi \cos \phi)}]. \quad (9)$$

Again the $e^{ikp(1 - \cos \psi \cos \phi)}$ term contributed by $P(0)$ introduces a time delay $(1 - \cos \psi \cos \phi) p/c$. With $p = 3000$ m, $\psi = 10^\circ$, and $\phi \sim -9.8^\circ$ this is 296 ns. The z_1 end of the transmission line starts affecting the V_{oc} at $z = 0$ at 296 ns after the incident wave reaches $z = 0$. The term is omitted if we restrict attention to the first 296 ns at $z = 0$. At these early times the open circuit voltage becomes

$$V(0) = -E_y^{inc}(h,0,0) d + \frac{A_1(\psi,\phi) d E^{inc}(h,0,0)}{1 - \cos \psi \cos \phi}. \quad (10)$$

Since E_y is $-E^{inc}(h,0,0) \sin \psi \sin \phi$ for vertical polarization and is $-E^{inc} \cos \phi$ for horizontal polarization, this voltage may be written as

$$V(0) = E^{inc}(h,0,0) d A(\psi,\phi) \quad (11)$$

where

$$A(\psi,\phi) = \begin{cases} \frac{\sin \psi \sin \phi}{1 - \cos \psi \cos \phi} & \text{vertical polarization} \\ \frac{\cos \psi + \cos \phi}{1 - \cos \psi \cos \phi} & \text{horizontal polarization.} \end{cases} \quad (12)$$

As discussed in Appendix B, this differs from Vance's directivity function,¹² that he evaluated for a single wire above a ground plane. The angular variations are shown in Figures 7 and 8 for the two polarizations. At given ψ in Figure 7, the peak occurs at $\phi = \psi$. The

term for vertical polarization is somewhat contrary to intuition. At $\psi = 90^\circ$, no magnetic flux threads the loop, and so zero coupling might be expected. However, $\phi = 90^\circ$ maximizes the E_y and its contribution dominates the voltage. At $\psi = 90^\circ$ in Eq (12) the vertical-polarization case degenerates to horizontal polarization. Yet $\sin \phi \neq \cos \phi$ for arbitrary values of ϕ . However, $\sin(90^\circ - \phi) = \cos \phi$, and the difference only reflects the definitions of horizontal and vertical polarization.

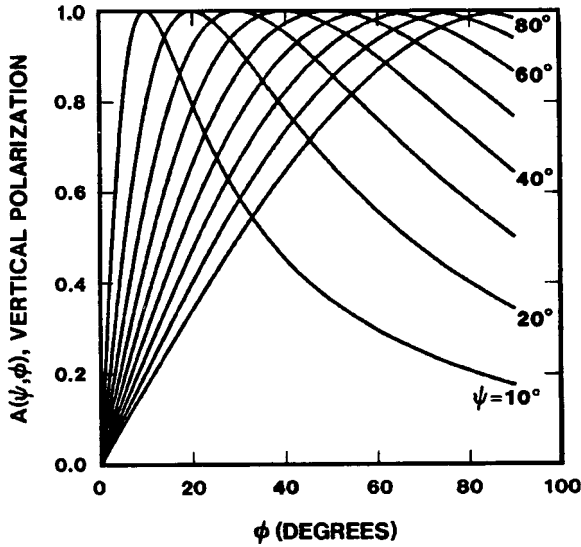


Figure 7. The angular factor $A(\psi, \phi)$ for transmission-line excitation by a vertically polarized incident wave

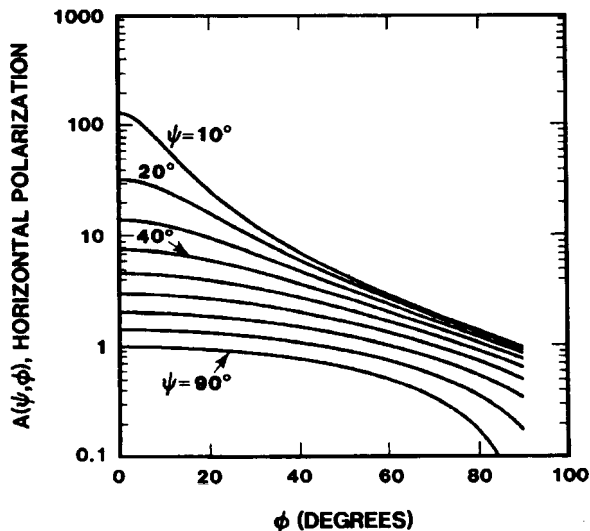


Figure 8. The angular factor $A(\psi, \phi)$ for transmission-line excitation by a horizontally polarized incident wave

The variation is more dramatic in Figure 8. The peak for horizontal polarization occurs at $\phi = 0$. At $\psi = 10^\circ$, the $\phi = 0$ gives a peak of 130; the peak falls to 14 at $\phi = 30^\circ$. The peak results from coherent addition of the transverse electromagnetic (TEM) signal propagating at speed c along the transmission line and the line excitation that travels at a phase velocity along the line that is $c/\cos \phi \cos \psi$. The closer the excitation and propagation speeds match, the greater the coherent addition. At $\psi = 0^\circ$ and $\phi = 0^\circ$, the large coupling for horizontal polarization should be modified by line and ground resistance effects that are neglected in Appendix B. The coupling is sensitive to the incident polarization.

4.3 Incident Polarization

The Starfish EMP incident on Honolulu had an elevation angle, $\psi = 10^\circ$. The azimuthal angle, ϕ (in Figure 6) is $\sim -9.8^\circ$. These parameters give the values $A(\psi, \phi) = -1$ for vertical polarization and 67 for horizontal polarization. For most incoming polarizations, the horizontal component dominates the coupling.

The incoming EMP is dominated by the magnetic dipole signal with its electric field in the $\mathbf{r} \times \mathbf{B}_g$ direction.¹³ The vector \mathbf{r} has the direction along the line of sight from the burst (Figure 1). \mathbf{B}_g is the ambient geomagnetic field in the gamma-ray absorption region. In our example, \mathbf{r} is tilted downward by 10° in a direction 54.3° east of magnetic north.¹¹ Within the EMP source region the geomagnetic dip angle and declination are $\sim 36^\circ$ and 11° E. In a local coordinate system at the observation point, with unit vectors \mathbf{e}_E , \mathbf{e}_N , \mathbf{e}_V in the east, north, and vertical directions, a unit vector in the direction of the magnetic field is approximated by $\mathbf{e}_B = \cos 36^\circ \cos 11^\circ \mathbf{e}_N + \cos 36^\circ \sin 11^\circ \mathbf{e}_E - \sin 36^\circ \mathbf{e}_V$. The unit vector along \mathbf{r} is $\mathbf{e}_r = \cos 10^\circ \sin 65.3^\circ \mathbf{e}_E + \cos 10^\circ \cos 65.3^\circ \mathbf{e}_N - \sin 10^\circ \mathbf{e}_V$. The cross product gives $\mathbf{e}_r \times \mathbf{e}_B = -0.104 \mathbf{e}_E + 0.499 \mathbf{e}_N + 0.647 \mathbf{e}_V$. The resulting angle between \mathbf{r} and \mathbf{B}_g is 59° . By taking the incident peak field as 5.6 kV/m from Figure 5, we find component peaks -0.71 , 3.39, and 4.40 kV/m in the east, north, and vertical directions. Although slightly smaller than the vertical component, the horizontal component, $(0.71^2 + 3.39^2)^{1/2} = 3.47$ kV/m, dominates because the $A(\psi, \phi)$ is much larger for this polarization.

4.4 Differential-Mode Voltage

The horizontal components in Eqs (2) through (7) exhibit a reduction in signal after the ground-reflected wave arrives. The time delay is $t_o = 2h \sin$

ψ/c ; that is, 9.5 ns for our problem where $h = 27 \text{ ft} = 8.23 \text{ m}$, $\psi = 10^\circ$. (Some might argue that 25 ft should be used, consistent with Figure 4. Our early information supported 27 ft. Masao Bentosino indicates that some poles did position the wire at 27 ft.) If the electric field rose linearly in time, then the V_{oc} would reach a peak after 9.5 ns and remain static until the linear rise was over. The peak electric field that is effective would be the maximum field change in 9.5 ns. This time interval is more restrictive than the earlier 296-ns constraint on the time.

Conversion of these equations to the time domain and restriction to a 9.5-ns time interval gives the open-circuit voltage from Eq (11). With horizontal and vertical components of $A(\psi, \phi)$ (at $\phi = -9.8^\circ$) being 67 and -1 , the differential voltage becomes

$$V_{oc} = 67 E_{ih}(t) d - E_{iv}(t) d.$$

The peak values $E_{ih} = 3.47 \text{ kV/m}$ and $E_{iv} = 4.40 \text{ kV/m}$, coupled with $d = 0.368 \text{ m}$, give $V_{oc}(\text{max}) = 84 \text{ kV}$. This clearly exceeds the cutout limits, 1000 to 1200 V, listed in Table 2. However, only a fraction of the 5.6 kV/m can influence the transmission line within the 9.5-ns window imposed by the ground reflection. The maximum field change that occurs within the window is $\sim 1.3 \text{ kV/m} \pm 10\%$ (as estimated from Figure 5). This gives $V_{oc} = 20 \text{ kV} \pm 10\%$. This example emphasizes the importance of rise time. A rise time $< 9 \text{ ns}$ would give a voltage drop over four times as large.

Consistent with the uncertainties involved, there are several variations that could be examined to alter the open-circuit voltage. If we were to include a realistic ground conductivity and permittivity, the reflected signal would be reduced, cancellation would be incomplete, and the effective E_i would increase slightly. The Z_2 could be given the more realistic value of Z_o , reducing the V_{oc} by a factor of ~ 2 . It is also possible that statistical variations in burn-through voltages in Table 2 allow some of the arcs to occur at voltages below the given lower limits. These limits are affected by the skill applied to the last filing of the cutout disk. Reflections and excitations from some of the discontinuities in Figure 2 could produce several pulses that propagate along the transmission line, giving increased possibilities for interference.

Choosing $Z_2 = Z_o$ rather than infinity, we find that our estimate of the voltage across the disk cutout becomes $V_{inc} = 10 \text{ kV}$. The estimated voltage is consistent with the observed effect being caused by EMP. Even allowing for this matched load at the fuse, the resulting voltage is sufficient to trigger the fuse.

These results leave one major contradiction to a convincing argument. If the induced voltage is so far above the value needed to produce the observed fuse closure, why wasn't the damage more extensive? Why weren't many more circuits upset? Rough estimates of RC time constants for the disk cutout (using transmission-line characteristic impedance for R) indicate response times of a few nanoseconds. So the fuses should respond quickly to the propagating signal; response time should not have limited the damage.

The idealized geometry of a single two-wire transmission line is expected to give an upper bound to the line voltage. Figure 2 suggests that rather than the propagating transmission-line voltage, the effective voltage charging the disk cutout is likely to be a smaller value. As a rough estimate, the junction at the disk cutout in Figure 2 might be viewed as a voltage divider. The propagating pulse would see three outgoing, two-wire transmission lines with the same 14.5-in. spacing. The equal characteristic impedances would reflect $\rho_i V_{inc}$ of the incident $V_{inc} = 10 \text{ kV}$, where $\rho_i = (3Z_o - Z_o)/(3Z_o + Z_o) = +1/2$. The transmitted voltage was divided by 3, giving 1700 V across the disk cutout. The corresponding transmission-line current is $1700 \text{ V}/Z_o$. From Appendix B, Z_o is $120 \ln(d/a) \Omega$. With $d = 0.368 \text{ m}$ and $a = 0.002058 \text{ m}$, $Z_o = 620 \Omega$ and the differential-mode peak transmission-line current that branched toward the disk cutout was 2.7 A.

The disk cutout is mounted on the crossarm that holds the streetlights, about 13 ft (4 m) below the isolation transformer. The geometry is indicated in Figure 9. The #8-gage wires are channeled inside a 1-in.-dia PVC pipe mounted along the pole and under the crossarm to the streetlight lines where the cutout is located. The incident peak of 1700 V sees the impedance discontinuity. A portion is reflected, leaving a smaller voltage incident on the parallel connection of the cutout and the PVC transmission line.

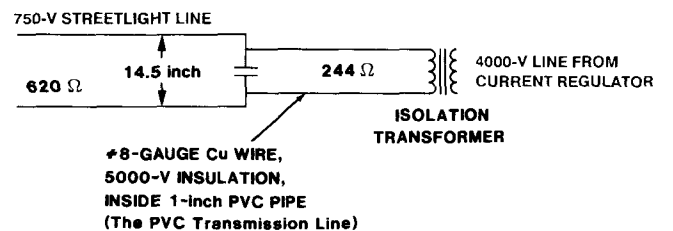


Figure 9. Transmission-line connections at the isolation-transformer disk cutout

Estimating the wire separation within the PVC pipe at 1/2 in. (1.27 cm), the characteristic impedance of the line is $Z_{PVC} = 120 \cosh^{-1}(d/2a) = 244 \Omega$. The

disk cutout might be approximated by two capacitors in parallel, with total capacitance $C = \epsilon_1 A_1/d_1 + \epsilon_2 A_2/d_2$. Here $d_1 = d_2 = 1.01$ mm. The $\epsilon_1 = \epsilon_0$ for the center (air) portion and $A_1 = \pi(3.2 \text{ mm})^2$. The insulator portion has the parameters $\epsilon_2 = 7 \epsilon_0$, $A_2 = \pi(7 \text{ mm})^2 - A_1$. This gives the estimate $C = 7.8$ pF. Thus the cutout appears as an open circuit for frequencies up to values such that $1/\omega C = 5Z_{\text{PVC}} = 1220 \Omega$, or $f \leq 16.7$ MHz. A few microhenries of lead inductance might cancel part of this reactance, but not enough to reduce the impedance at the parallel connection much below 244 Ω .

The propagating 1700 V experiences an impedance mismatch from 620 Ω to 244 Ω , giving a reflection coefficient of -0.44 . The transmitted voltage, incident on the disk cutout then has a peak value of $1700(0.56) = 950$ V. With the failure levels of 1000 to 1200 V in Table 2, **this is a feasible damage mechanism. The threat is at the threshold for damage, consistent with damage to only a few circuits.** Circuit orientation that results in a voltage adding to the instantaneous value of the 750-V, 60-Hz signal furnished by the current regulator can also restrict damage to a subset of the susceptible circuits. Detailed modeling of the junction might also include the incident fields interacting with the added sections of the transmission line and the common-mode excitation of the line. Contributions from the added sections will lack the coherent buildup and are expected to be small correction terms. The common-mode excitation must be considered to understand the threat to the individual streetlights.

4.5 Common-Mode Signals

At line locations before the junction, where the propagating voltage is ~ 10 kV, the differential-mode current is ~ 16 A. This is too large for lamp filaments. An estimate of the peak current in the streetlights must include the common-mode signal. The more detailed examination that was suggested to quantify the thick transmission-line effects would also note that the wiring diagram in Figure 2 does not suggest a balanced transmission line. The 30 lamps have a total resistance of $30 \times 25 \text{ V}/6.6 \text{ A} = 114 \Omega$. The characteristic impedance of the differential mode is $\sim 620 \Omega$. The unequal distribution of streetlights unbalances the line.

The incident electric field discussed earlier results in an incident magnetic field with mainly vertical and southward components. The vertically upward component induces a differential-mode current in a clockwise direction (Figure 6). The common-mode current is in the $+z$ direction; hence the peak

current carried by a streetlight assembly in this leg is the difference between the common-mode and differential-mode peak currents: $I_T = I_c - I$. The total current (including the utility contribution that could be up to 6.6 A in either direction) must be < 13.2 A (at least for a resistive streetlight assembly) because otherwise some of the individual-lamp cutouts would have fired. Because lamps are located in both legs, this limits the current in both legs of the transmission line.

Lee [Ref. 12, p 377] gives the early-time response of an isolated, infinitely long conductor of radius R_o in free space. (Here the $e^{+j\omega t}$ convention is used, as in Reference 12.)

$$I_c(z, \omega) = \frac{4E^i(\omega) e^{-jkz \cos \theta}}{k \sin \theta Z_o H_o^{(2)}(kR_o \sin \theta)},$$

where $k = \omega/c$, $E^i(\omega)$ is the incident electric field, $Z_o = 377 \Omega$, and θ is the angle between the propagation vector and the line axis. The magnetic field of the incident wave is perpendicular to the wire. Because our isolation transformer is over 200 m from the $z = -p$ end of the transmission line, and because we are interested in a 9.5-ns window of the signal (corresponding to a propagation distance of 2.8 m), the line can be treated as infinitely long. From Figure 6 with $\psi = 10^\circ$ and $\phi = -9.8^\circ$, we find $\theta = 13.6^\circ$. The small $kR_o \sin \theta$ allows the Hankel function to be approximated to give

$$I_c(z, \omega) = \frac{-2\pi c E^i(\omega) e^{-jkz \cos \theta}}{Z_o \sin \theta j\omega \ln(kR_o \sin \theta)}.$$

The conductor radius is chosen as 2.058 mm, appropriate for the #6 gage wire used in the streetlight circuits.⁸ The resistance per unit length is 1.3 Ω/km at 20°C and is neglected here. Since the coupling is actually to two wires, use of one gives an upper limit to the portion of the common-mode current in that one wire. The scattered fields from the second wire will cancel part of the original current.

The slowly varying \ln term can be approximated as a constant to obtain a quick upper limit for I_c . $kR_o \sin 13.2^\circ = 1.57 \times 10^{-12} \omega$. If we choose ω to represent the 38-ns rise time in our incident pulse, $\omega \approx 1.65 \times 10^8/\text{s}$ and the \ln factor is -8.26 . If we choose ω to represent the full width at half maximum for our incident pulse, $\omega \approx 1.9 \times 10^7/\text{s}$, the \ln factor becomes -10.42 . During the rise of the incident pulse the

–8.26 factor is more appropriate. The common-mode current becomes (in SI units)

$$I_c(z,\omega) = 2.7 \times 10^6 \frac{E^i(\omega)}{j\omega} e^{-jkz \cos \theta}.$$

Conversion to the time domain gives

$$I_c(z,t) = 2.7 \times 10^6 \int_0^t E^i\left(t' - \frac{z \cos \theta}{c}\right) dt'.$$

Within the 9.5-ns time window before ground reflections arrive, the E^i rises nearly linearly with time. The maximum field change within this window is 1.3 kV/m. If the polarization were such that the incoming magnetic field is orthogonal to the wire, then the full 1.3 kV/m can be used.

The unit vector in the wire (z) direction is $\mathbf{e}_z = \sin 56^\circ \mathbf{e}_E + \cos 56^\circ \mathbf{e}_N = 0.829 \mathbf{e}_E + 0.559 \mathbf{e}_N$. The unit vector in the direction of E^{inc} was found earlier as $\mathbf{e}_{E^{\text{inc}}} = -0.126 \mathbf{e}_E + 0.606 \mathbf{e}_N + 0.785 \mathbf{e}_V$. The unit vector in the direction \mathbf{k} is the \mathbf{e}_r found earlier, $\mathbf{e}_r = 0.895 \mathbf{e}_E + 0.412 \mathbf{e}_N - 0.174 \mathbf{e}_V$. Thus the unit vector in the direction of incident magnetic field is

$$\begin{aligned} \mathbf{e}_B &= \mathbf{e}_r \times \mathbf{e}_{E^{\text{inc}}} = 0.429 \mathbf{e}_E - 0.681 \mathbf{e}_N \\ &+ 0.594 \mathbf{e}_V. \end{aligned}$$

The inner product of the unit vectors \mathbf{e}_z and \mathbf{e}_B indicates that these vectors are 91.4° apart. The incident magnetic field is within 2° of being orthogonal to the wire, maximizing this type of coupling.

Using the full 1.3 kV/m and a linear rise gives the peak common-mode current at 9.5 ns; $I_c = 16.7$ A. At the line location where $Z_0 = 620 \Omega$ and the propagating peak voltage is 10 kV, the peak differential current is 16 A. This limit gives $16.7 - 16 = 0.7$ A on the transformer leg and $16.7 + 16 = 32$ A on the other leg in Figure 2.

A better approximation to the peak common-mode current is found by letting the integral extend beyond 9.5 ns. The first 9.5 ns of the incident pulse is taken as the $5600 \text{ V/m} \sin[26.624 t(\mu\text{s})]$ variation suggested for the rise in Figure 5. After a delay of 9.5 ns, the same pulse is subtracted, with the t replaced by $t - 9.5$ ns. At $t \geq 63.75$ ns the sum is taken as zero. The resulting pulse is illustrated in Figure 10. It represents a driving field with reasonable horizontal electric fields to include reflection effects (from a perfect reflection at the ground). Using the integral of this E^i out to 64 ns indicates that the peak

common-mode current is ~ 140 A. This value is consistent with estimates from the TWTD computer code,¹⁴⁻¹⁵ where current pulse widths were ~ 200 ns. **Common-mode currents dominate those from differential-mode excitation.** With such large currents in a circuit designed for 6.6 A, the streetlights themselves might suffer damage. The individual lamp cutouts were expected to start failing for current > 13.2 A.

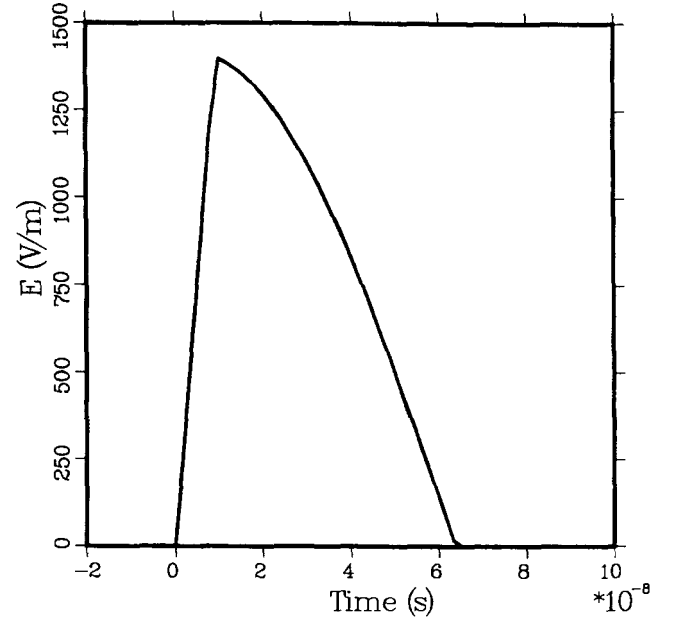


Figure 10. Incident EMP (at $\psi = 10^\circ$) that provides a horizontal component of electric field that includes the reflected-pulse contribution

4.6 Streetlight Survival

During normal operation the individual streetlights carried 6.6 A with a 22-V drop across each 2500-lumen lamp. This indicates that the lamp-assembly had a 150-W bulb with a 3.3- Ω , 60-Hz resistance at operating temperature. Measurements on two samples of lamp cutouts indicate a $C \sim 15$ pF. At high enough frequencies the cutout will act as a shunt and limit the voltage drop. However, for $1/\omega C$ to reach 3.3 Ω and halve the voltage drop from a large line current, the frequency must be 3.2 GHz. This is clearly not the mechanism that protects the streetlights.

The streetlight assembly has a 2.2- by 7-cm clamp that holds the disk cutout. The clamp has an average separation of ~ 5 mm, giving an effective capacitance closer to $C = 15 \text{ pF} + \epsilon_0(2.2 \times 7 \times 10^{-4})/5 \times 10^{-3} = 18 \text{ pF}$. This is still not enough to form an effective shunt. Impedance measurements of the streetlight assembly that includes the lamp, its socket and the disk cutout are illustrated in Figures 11 and 12. The

resistance stays below 1 Ω . It is assumed that at operating temperature this resistance rises to $\sim 3.3 \Omega$. The reactance remains inductive throughout the measurements shown in Figure 12. Division by ω gives the effective inductance shown in Figure 13. The L is roughly 1 μH .

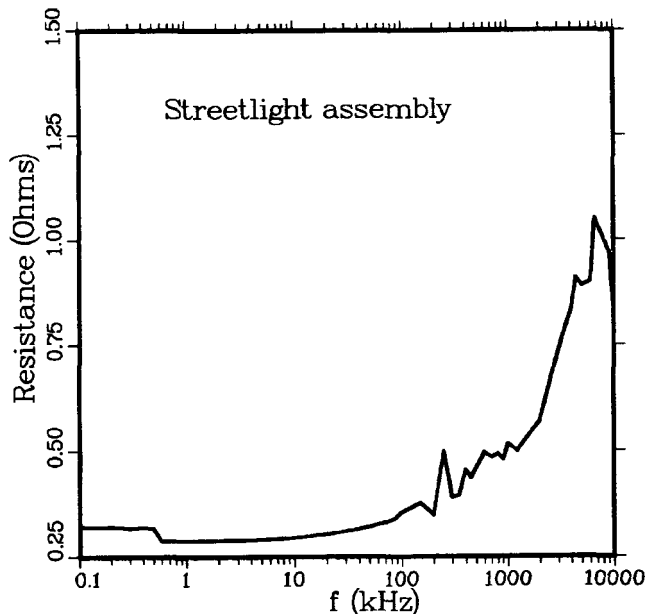


Figure 11. Real part of the streetlight-assembly impedance

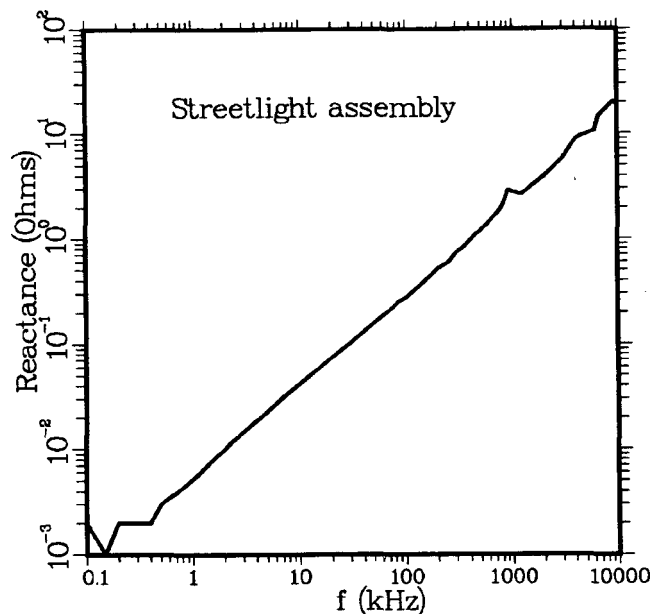


Figure 12. Imaginary part of the streetlight-assembly impedance

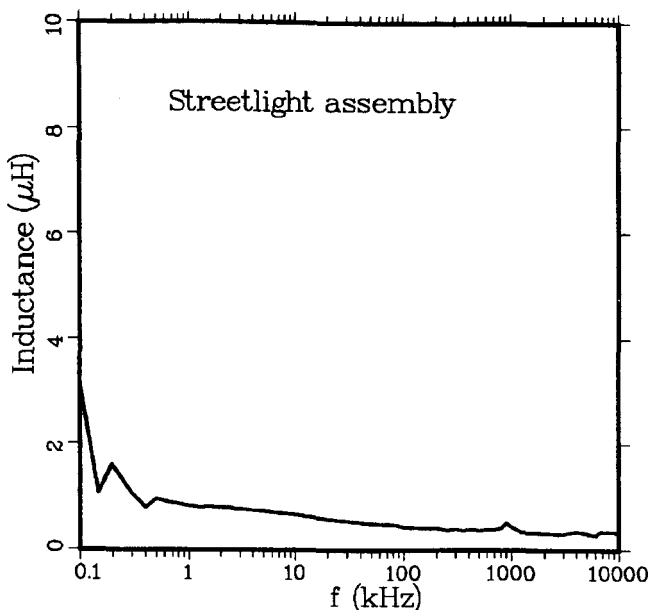


Figure 13. Effective inductance of the streetlight assembly

It is estimated that leads going from the streetlight assembly to the streetlight lines added another 2 μH (as estimated from the high-frequency inductance of a straight wire, $L = 2\ell[\ln(2\ell/a) - 3/4] \times 10^{-7}$, $\ell = 2 \text{ m}$ and #6-gage wire). Thus the impedance presented by the streetlights is not small compared to the 3.3- Ω low-frequency value and 140 A through the streetlights should cause at least some of those disk cutouts to fail.

Another mechanism that might explain the survival of the streetlight cutouts is that a high streetlight impedance limited the line currents on the streetlight leg. At a surge frequency $\sim 4 \text{ MHz}$ and $L = 3 \mu\text{H}$, the streetlight reactance is 75 Ω , already large compared to its resistance and large compared to the local impedance of neighboring parallel wires (illustrated in Figure 4). Checking this requires more involved coupling codes. A simpler possibility is that the voltage rating of the disk cutouts is not to be trusted. This possibility was tested by Sam Holmes and George Seely at SNL, who exposed 12 disk cutouts (for the 4000- and 6000-lumen lamps) to 100-ns and 500-ns pulses at 1 kV. This voltage was 5 times the cutouts' maximum rated level. No damage occurred. The individual streetlight cutouts did not respond fast enough for a 140-A, 200-ns common-mode current pulse to damage the streetlight cutouts.

In spite of the voltage drops across the streetlights that are estimated from common-mode currents being much greater than the rating of their protective cutouts, the streetlight survival is consistent with expectations.

4.7 Additional Hardware Considerations

The lighting geometry diagrammed in Figures 2, 3, and 6 is idealized from that actually encountered in 1962. Figure 4 shows some of the neighboring wires that were likely to be present. Such neighbors help share the common-mode current, reducing that threat with no significant effect on the differential-mode voltage that caused the experienced damage.

Examination of the 1988 system indicates that even the geometry suggested by Figure 4 is an ideal-

ization. Figure 14 shows a view toward the southeast taken from the deadend at Aleo in Figure 2. A modern streetlight is seen at the top of this July 1988 photograph. Less visible are the streetlights on the third and fifth telephone poles as you proceed along Aleo. The street between the third and fourth poles is Ferdinand. The streetlights seem to be arranged as they were in 1962 (illustrated in Figure 2). On close examination the poles show considerable wear; 25 years of service seem possible. Just beyond the third streetlight is where the isolation transformer and its disk cutout were located in 1962. Extra wires are present that are not accounted for in the analysis. Extra wires in 1962 cannot be accounted for.

Figure 15 illustrates the view along Ferdinand Street toward Johnston Atoll. The stop sign is at the Aleo intersection. The gentle slope suggests that the elevation angle (with respect to the ground) was



Figure 14. View along Aleo, southeast, toward Ferdinand

larger than 10° . Some line drooping is also apparent between the poles. The wiring does appear more idealized than at the intersection and perhaps is able to support the coherent addition necessary for the cutout damage.

One of the 1962-type streetlights with its 2500-lumen bulb is illustrated in Figure 16. The pipe was mounted to a telephone pole. Two glass insulators show where the series connections were made to the #6-gage streetlight wires. About 2 m of wire were necessary to make these connections. Such streetlights offered perturbations in the idealized geometry that gave the coherent signal propagating toward the isolation transformer and its disk cutout. These hardware considerations indicate some features of the 1962 system that have not been rigorously taken into account.



Figure 15. View along Ferdinand toward the Aleo intersection and toward Johnston Atoll

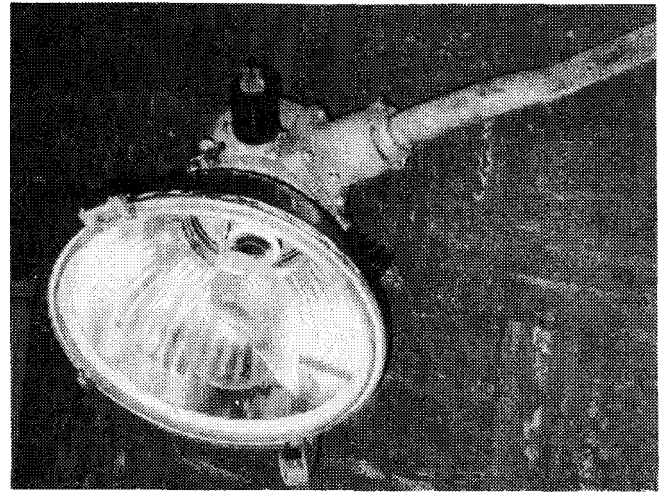


Figure 16. A 2500-lumen streetlight of the type used in 1962

4.8 Energy Balance for Disk-Cutout Failure

To contribute to damage, the EMP energy propagated in the differential mode in the 244- Ω , 13-ft-long PVC line. Earlier we estimated this peak voltage at 950 V. The time dependence followed the dominant horizontal component of incident electric field (Figure 10). The spark might have occurred at the peak, so the following portion of the incident voltage contributed to the local heating and permanent damage. The following pulse width at half-maximum was ~ 30 ns. It is likely that the disk-cutout load was not matched throughout the pulse. However, if all of that energy was absorbed by the lead near the position of the spark, then we obtain the first row in Table 4. Any reflected energy increased the resistance and gave a less-effective short.

The energy available in Table 4 was estimated as one-half the $V_{\text{peak}} I_{\text{peak}}$ times the time interval, based on the differential-mode voltage and current having

the same waveshape. The melt mass (m_m) in the table resulted from the 15 cal/g enthalpy to melt for disk-cutout lead starting at room temperature. This mass assumed that all the available energy goes into the melted lead. The 11 g/cm³ lead density fixed the radius of a lead cylinder, 40 mil (1.02 mm, the cutout gap) long, that had mass m_m . This cylinder radius is also listed in Table 4. The 19.8×10^{-8} Ω -m resistivity for lead determined the resistance of that cylinder. The resulting rough estimate for the cylinder resistance indicated that the resistance provided an effective short for the 244- Ω PVC line and caused the streetlights to go out.

When the spark occurred (at ~ 1200 V) the current provided by the isolation transformer was also shorted across the cutout. There the current might have been as high as $3.9 + 6.6 = 10.5$ A, as indicated in the second row of Table 4. If we assume that the spark lasted the same 30-ns time interval at the limiting voltage 1200 V, the resulting cylinder resistance was 0.75 Ω . This gave a slightly more effective short.

As the isolation transformer continued to generate 6.6 A through the 0.75 Ω , $I^2R = 33$ W, or 7.8 cal/s. The energy absorption was concentrated where the spark originally occurred. At this I^2R rate of energy absorption, 1 g of lead could be melted in 2 s. The mass of two lead disks in a cutout is ~ 8.1 g, but only a small fraction melted at failure.

Heat conduction diverted a portion of the energy from melting the lead. The thermal conductivity of lead is 0.083 cal cm/s/cm²/°C. The melted lead was at 327°C. With a temperature difference 300°C across 1 cm, the rate of heat flow would be 25 cal/s/cm². So the 7.8 cal/s heating rate soon raised the 8-g lead mass to a high temperature. More lead melted until the I^2R was low enough to be dissipated by conduction, convection, and radiation from the cutout. Most of the melt energy was provided by the isolation transformer rather than by the incident EMP.

The resistances in Table 4 are also underestimated because a portion of the PVC-line excitation is reflected by the unmatched load at the cutout. This reinforces the conclusion that power from the transformer itself contributed to the permanent damage.

Table 4. Estimate of cutout resistance after failure

Peak Voltage (V)	Peak Current (A)	Time Interval (ns)	Energy Available (μ J)	Melt Mass (μ g)	Cylinder Radius (μ m)	Cylinder Resistance (Ω)
950	3.9	30	56	0.89	5.0	2.6
1200	10.5	30	189	3.0	9.2	0.75

5. Conclusions

Because of the hardware considerations that have been noted, we cannot claim to have a rigorous analysis of the 1962 Hawaiian streetlight incident. Unknowns in the complications caused by neighboring wires and lack of circuit details for 1962 prevent a rigorous analysis today. Such data as "How many clear-plastic washers were in the transformer cutouts that failed?" are not now available. Nevertheless, a consistent view has emerged. That view is supported by the limited analysis.

The damaged streetlight circuit had several characteristics that enhanced its vulnerability to the Starfish EMP. The line-voltage rating was at its upper electrical-code limit (750 V) for that pole position. The circuit orientation was near the maximum for differential coupling to the horizontal component of the incident electric field. The incident magnetic field was within 2° of being orthogonal to the wires, maximizing common-mode coupling to the line.

The basic factor limiting the transmission-line voltage was the canceling effects of the ground-reflected signal. A faster rise in the EMP, a higher peak EMP value, or a further delay in arrival of

reflected signals would have caused increased voltage and produced more failures. The estimated differential-mode voltages are enough to have caused the observed damage. Orientation effects, expected discontinuities in the transmission lines, and the interaction between differential-mode and common-mode excitations make the present estimates consistent with damage occurring in only a portion of the strings in the system and consistent with none of the individual streetlights being damaged. Even though common-mode currents dominate those from differential-mode excitation and are large enough to exceed streetlight-cutout survival levels, the slow response of the streetlight-cutouts allowed them all to survive.

This analysis gives a basis for attributing the cutout damage to an EMP effect and supports earlier claims of EMP effects on the Hawaiian streetlights.² The photoelectric cells are in a 2400-V utility distribution circuit that is more difficult to upset than the failed 750-V lighting circuit and is difficult to excite in a way that produces the observed damage.

References

- ¹F. M. Tesche, *IEEE Trans on Power Delivery*, PWRD-2,1213(1987). The effects were reported earlier by G. S. Parks, Jr., T. I. Dayharsh, and A. L. Whitson, *A Survey of EMP Effects During Operation Fishbowl*, DASA Report DASA-2415, May 1970 (SRD).
- ²S. Glasstone and P. J. Dolan, *The Effects of Nuclear Weapons*, US DoD and US DOE, 1977. Their source was likely to be Parks et al. in our Reference 1 and ultimately the Watson reports in Reference 6.
- ³M. Rabinowitz, *IEEE Trans on Power Delivery*, PWRD-2,1199(1987).
- ⁴C. N. Vittitoe, *IEEE Trans on Power Delivery*, PWRD-2,1209(1987).
- ⁵John Mattox, *Bull Am Phys Soc* 30:392(1985) and his associated notes.
- ⁶J. Watson, memoranda identified only as 00333/00334 of Lawrence Livermore National Laboratory. My copies of the notes are not dated and are not clearly identified. Wouters indicated that Watson died shortly after the notes were written. Reference copies of the memoranda may not be available.
- ⁷In a 1988 interview, to obtain a value for the voltage across a lamp, Willy Souza referred to the *Lineman's and Cableman's Handbook*, by E. B. Kurtz, McGraw Hill, NY, 1955. There the lamps were described as requiring 6.6 A, 22 V to give the rated 2500 lumens. However, at intersections or other areas where more light was required, 4000-lumen or 6000-lumen lamps were used. These lamps required 34.2 V and 50.5 V, respectively. We use 25 V per lamp for our estimates. The #6-gage copper lines were held to the crossarms by mounting to glass insulators.
- ⁸D. G. Fink and H. W. Beaty, *Standard Handbook for Electrical Engineers*, 11th Ed, McGraw Hill, 1978, p18-44; see Table 18-6, Typical Characteristics of Single Phase and 3-Phase 60-Hz Distribution Transformers. The 5-kVA transformers typically have 2.2% IR, 2.2% IX, 3.1% IZ, 0.72% no-load loss, and 2.04% Cu loss. (These numbers vary slightly with the voltage rating.)
- ⁹C. N. Vittitoe, "Did High-Altitude EMP Cause the Hawaiian Streetlight Incident?," presentation at US-Japan Seminar on Electromagnetic Interference in Highly Advanced Social Systems, August 1-4, 1988, Sandia National Laboratories Conference Report No. SAND88-0043C.
- ¹⁰J. S. Malik of Los Alamos National Laboratory attributes this early speculation to Don Shuster while Shuster was at Sandia National Laboratories, private communication, 1987; verified by D. Shuster, private communication, 1988.
- ¹¹C. L. Longmire, *EMP on Honolulu from the Starfish Event*, EMP Theoretical Note 353, March 1985. Also see *Bull Am Phys Soc* 30:392 (1985).
- ¹²E. F. Vance, *Coupling to Shielded Cables*, Wiley, 1978. For a general discussion of EMP interactions, see K. S. H. Lee, Ed, *EMP Interaction: Principles, Techniques and Reference Data (A Handbook of Technology from the EMP Interaction Notes)*, Hemisphere Publishing Corporation, New York (distributed also by Springer-Verlag, Tokyo) 1986.
- ¹³C. L. Longmire, R. M. Hamilton, and J. M. Hahn, *A Nominal Set of High-Altitude EMP Environments*, EMP Theoretical Note 354, January 1987.
- ¹⁴M. Van Blaricum and E. K. Miller, *TWTD: A Computer Program for the Time-Domain Analysis of Thin-Wire Structures*, UCRL-51277, October 28, 1972.
- ¹⁵J. A. Landt, E. K. Miller, and F. J. Deadrick, *Time-Domain Computer Models of Thin-Wire Antennas and Scatterers*, UCRL-74848, November 1973.

APPENDIX A

Isolation-Transformer Impedance

The transformer supplied by Masao Bentosino and the Honolulu Streetlight Department would have been a critical part of the analysis except for two mitigating factors. The transformer has a 2-kVA rating rather than 5 kVA, and the disk cutout was separated from the transformer by a 13-ft-long transmission line. The first factor could be overcome by scaling the transformer data. However, the second factor separates the signal into an incident portion and a portion reflected at the transformer and arriving ~ 26 ns later. This separation is longer than the 9.5-ns delay for arrival of the ground-reflected signal

that reduces the excitation. Transformer data are presented here in case a more detailed analysis is attempted later.

The transformer has identification markings: Westinghouse WP 17932-B, Style 1566974-D. Measurements of the real and imaginary portions of the secondary impedance are illustrated in Figures A-1 to A-2. The data were taken by N. I. Turner at Sandia National Laboratories, with a Hewlett Packard Model 4192A Impedance Analyzer. The data were recorded at room temperature, not at the usual transformer operating temperature.

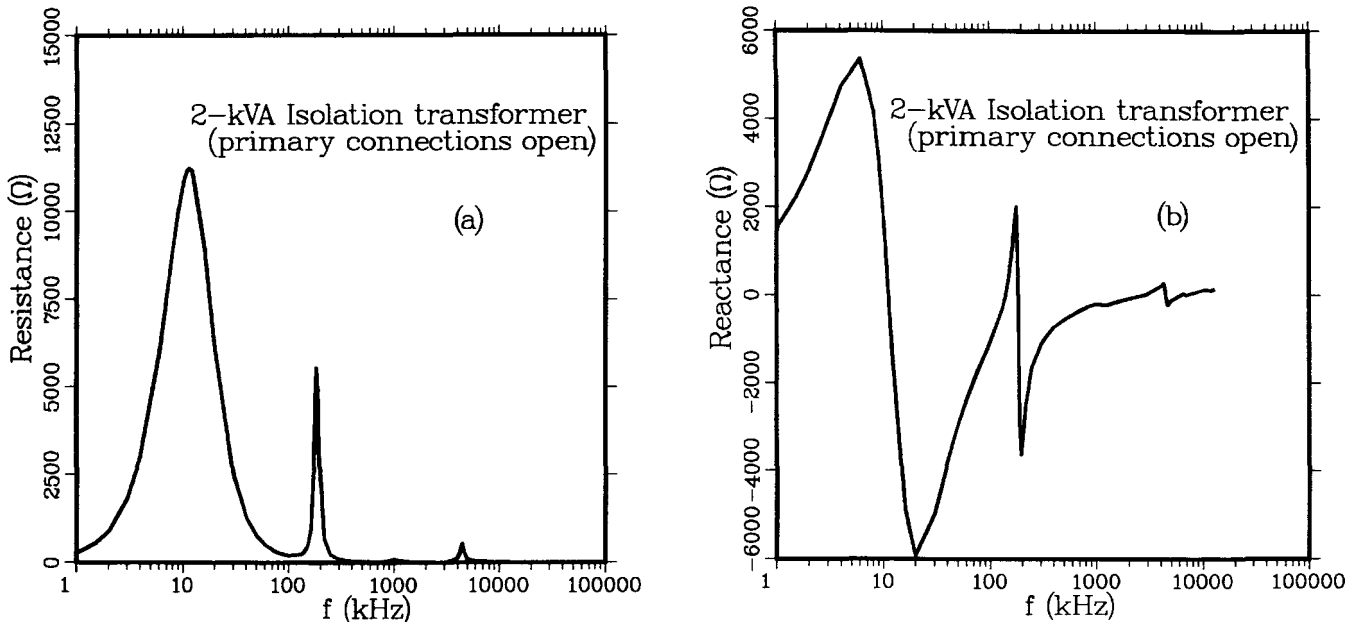


Figure A-1. Real (a) and imaginary (b) parts of impedance of the secondary winding, with the primary connections open

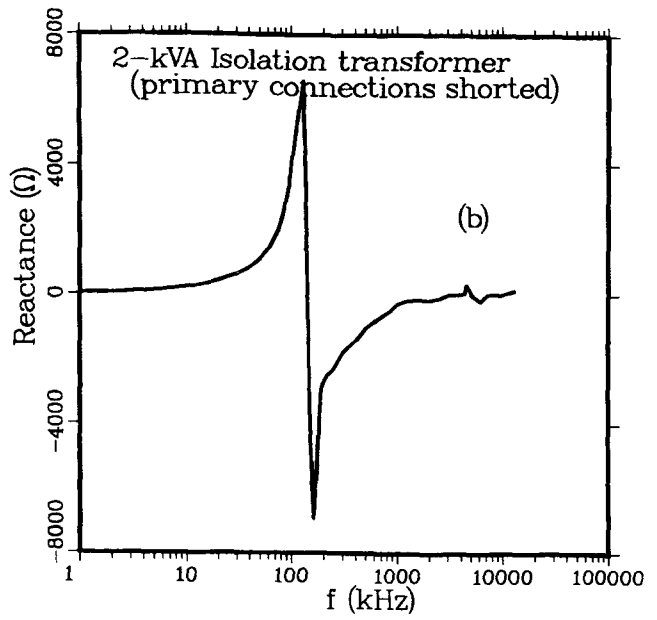
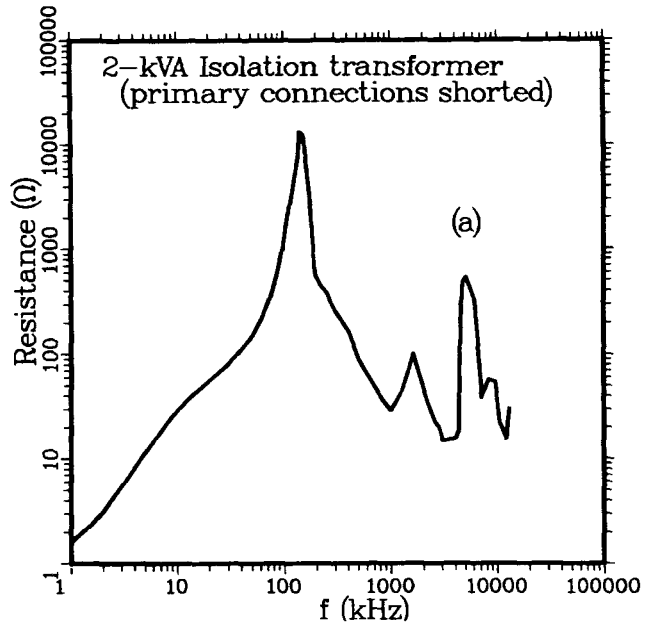


Figure A-2. Real (a) and imaginary (b) parts of impedance of the secondary winding, with the primary connections shorted

APPENDIX B

Plane-Wave Excitation of a Two-Wire Transmission Line

B.1 Geometric Line Parameters

The transmission line consists of two wires of radius, a , separated by distance, d , with $d/2a \gg 1$. Both a and d are small compared to the line length, p . We assume that only TEM line modes are significant and that wavelengths are long enough so that the line and ground losses can be ignored and that the static forms of capacitance, C , and inductance, L , per unit length are appropriate. The C and L are given by^{B-1}

$$C = \frac{\pi\epsilon_0}{\cosh^{-1}(d/2a)},$$

$$L_{\text{external}} = \frac{\mu_0}{\pi} \cosh^{-1}(d/2a).$$

These parameters have the property that $CL = 1/c^2$.

The line impedance per unit length is $Z = R - i\omega L$, where the time dependence $e^{-i\omega t}$ is assumed and where R is the line resistance per unit length. The shunt admittance per unit length is $Y = G - i\omega C$. The characteristic impedance is defined as $Z_0 = (Z/Y)^{1/2}$. The current density and conductivity in the medium surrounding the wires are assumed to be zero.

Ignoring line losses ($R = 0$) and shunt conductance ($G = 0$) gives $Z = -i\omega L$ and $Y = -i\omega C$. For this idealized line, $Z/Y = L/C = Z_0^2$, $Z/Z_0 = -ik$, and the characteristic impedance becomes $Z_0 = (L/C)^{1/2} = (\mu_0/\epsilon_0)^{1/2} \cosh^{-1}(d/2a)/\pi$. Since $d \gg 2a$, $Z_0 = 120 \Omega \ln(d/a)$.

B.2 Transverse Driver

The diagram in Figure B-1 represents plane-wave excitation of the simple transmission line. The line is at height h above ground, with its plane parallel to the ground. We assume that the wires are thin so that the transmission line supports only the TEM propagation mode and does not reradiate enough to affect the coupling. At all frequencies of interest, currents flow only in the longitudinal direction; no circumferential flow occurs. These assumptions decouple the propagation problem from the excitation problem. When the wire geometry is thick, so that the wire does influence the excitation (as at the discontinuities in Figure 2), more involved procedures are needed for a rigorous treatment.^{B-2}

Consistent with our transmission-line assumptions that allow neglect of the vector-potential time variation, the line voltage at position z is given by

$$V(z) = - \int_0^d \mathbf{E}_y(h,y,z) dy.$$

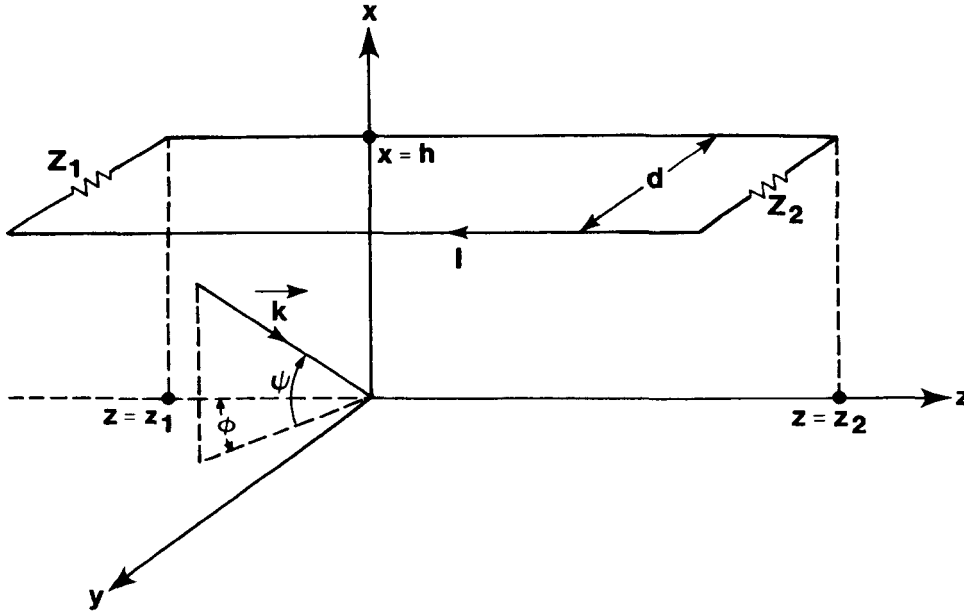


Figure B-1. Incident-wave geometry for the transmission line

Ampere's law coupled with the $e^{-i\omega t}$ time dependence gives

$$E_y = \frac{i\omega}{K^2} \frac{\partial B_z}{\partial x} - \frac{i\omega}{k^2} \frac{\partial B_z}{\partial x},$$

where

$$k = \omega/c \text{ and}$$

$$c = (\mu_0 \epsilon_0)^{-1/2}.$$

Following work by Taylor, Satterwhite, and Harrison,^{B-3} we separate \mathbf{B} into incident and scattered components, and find

$$V(z) = -\frac{i\omega}{k^2} \frac{\partial}{\partial z} \left[\int_0^d B_x^{inc}(h,y,z) dy + \int_0^d B_x^{sc}(h,y,z) dy \right] + \frac{i\omega}{k^2} \frac{\partial}{\partial x} \int_0^d B_z^{inc} dy.$$

The scattered magnetic field has no z component; the scattering produces current in the line that provides B_x and B_y components, but not B_z .

Figure B-1 illustrates the wave vector \mathbf{k} for the incident plane wave. The incident wave has field components orthogonal to \mathbf{k} that are represented by an amplitude modulated by $\exp(i\mathbf{k} \cdot \mathbf{x} - i\omega t)$. With the components $k_x = -k \sin \psi$, $k_y = -k \cos \psi \sin \phi$, $k_z = k \cos \psi \cos \phi$, and with

$$LI = \int_0^d B_x^{sc}(h,y,z) dy$$

(where L is the inductance per unit length), the voltage becomes

$$V(z) = c \cos \psi \cos \phi \int_0^d B_x^{\text{inc}} dy - \frac{i\omega L}{k^2} \frac{\partial I}{\partial z} + c \sin \psi \int_0^d B_z^{\text{inc}} dy.$$

Since $L = 1/Cc^2$, and $-i\omega L/k^2 = -1/Y$, this equation becomes

$$\frac{\partial I}{\partial z} + YV(z) = Y \left[\cos \psi \cos \phi \int_0^d c B_x^{\text{inc}} dy + \sin \psi \int_0^d c B_z^{\text{inc}} dy \right]. \quad (\text{B-1})$$

The vertical polarization in Figure B-1 has the incident electric-field amplitude in a vertical plane, orthogonal to \mathbf{k} . In this case the components of \mathbf{B} are $B_x^{\text{inc}} = 0$, $B_y^{\text{inc}} = B^{\text{inc}} \cos \phi$, $B_z^{\text{inc}} = B^{\text{inc}} \sin \phi$. Since $cB^{\text{inc}} = E^{\text{inc}}$ and $E_y = -E^{\text{inc}} \sin \psi \sin \phi$, Eq (B-1) becomes our first transmission-line equation.

$$\frac{dI}{dz} + YV(z) = -Y \int_0^d E_y^{\text{inc}}(h,y,z) dy. \quad (\text{B-2})$$

For the case of horizontal polarization, the incident magnetic-field amplitude is in a vertical plane, orthogonal to \mathbf{k} . The corresponding components of \mathbf{B} are $B_x^{\text{inc}} = B^{\text{inc}} \cos \psi$, $B_y^{\text{inc}} = -B^{\text{inc}} \sin \psi \sin \phi$, and $B_z^{\text{inc}} = B^{\text{inc}} \sin \psi \cos \phi$, while $E_y = -E^{\text{inc}} \cos \phi$. Substitution of these components into Eq (B-1) again yields Eq (B-2). The E_y^{inc} is the driver for a voltage source distributed along the transmission line.

B.3 Longitudinal Driver

Figure B-2 gives the circuit diagram for a section of the simple transmission line. The transverse driving term $E_y^{\text{inc}} dy$ is inserted as a distributed voltage source (as an alternate interpretation to the short-circuit current driver chosen elsewhere).^{B-4}

The longitudinal driver is evaluated from Faraday's law of electromagnetic induction.

$\oint \mathbf{E} \cdot d\boldsymbol{\ell} = -\frac{\partial}{\partial t} \int \mathbf{B} \cdot \mathbf{n} da$. Following the path around the element dz in Figure B-2 gives

$$V(z+dz) - V(z) = Z_1^i \int_z^{z+dz} (I_2 - I_1) dz' = \partial/\partial t \int_0^d B_x(y,z) dy dz.$$

Z_1^i is the intrinsic impedance per unit length for each of the two wires in the line. As indicated by Taylor et al.,^{B-3} the differential-mode current is retrieved by letting $I_2 = I_c + I$, $I_1 = I_c - I$, $Z_1^i = 2Z_1^i$ so that

$$\partial V/\partial z + Z^i I = \partial/\partial t \int_0^d B_x(y,z) dy.$$

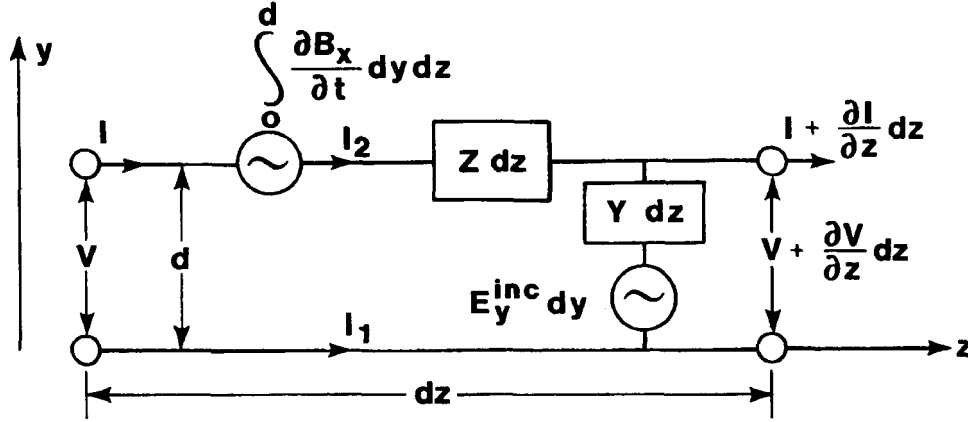


Figure B-2. Circuit diagram for a section of the transmission line

Separation of B_x into incident and scattered components as before yields

$$\frac{\partial V}{\partial z} + ZI = \frac{\partial}{\partial t} \int_0^d B_x^{\text{inc}}(y,z) dy, \quad (\text{B-3})$$

where

$$Z = Z^i - i\omega L.$$

Equation (B-3) is the second of the transmission-line equations.

The longitudinal driver is the integral term in Eq (B-3), as also indicated in Figure B-2. It is not correct to interpret the longitudinal driver per unit length as E_z , as suggested by Vance.^{B-5} As was the case for Eq (B-1), the driving term in Eq (B-3) can be written in terms of the incident electric field. However, the result differs for the two incident polarizations. With vertical polarization, $B_x^{\text{inc}} = 0$, giving

$$\frac{\partial V}{\partial z} + ZI = 0 \quad (\text{vertical polarization}). \quad (\text{B-4})$$

Horizontal polarization has $B_x = B^{\text{inc}} \cos \psi$, and so Eq (B-3) becomes

$$\frac{\partial V}{\partial z} + ZI = -ik \cos \psi \int_0^d E^{\text{inc}}(y,z) dy \quad (\text{horizontal polarization}). \quad (\text{B-5})$$

B.4 Solution of the Transmission-Line Equations

The transmission-line equations are:

$$\frac{\partial V}{\partial z} + ZI = E_z^{(s)}, \quad (\text{B-6})$$

$$dI/dz + YV(z) = -YV_y^{(s)}. \quad (\text{B-7})$$

Equation (B-2) identifies $V_y^{(s)}$ as

$$V_y^{(s)}(z) = - \int_0^d E_y^{\text{inc}}(h,y,z) dy . \quad (\text{B-8})$$

In our application, $k_y = -k \cos \psi \sin \phi$, where ψ is near 10° and ϕ is -9.8° . For frequencies and for wire separations, d , so that the restriction

$$k_y d = \omega \cos \psi |\sin \phi| / c \ll 1 \quad (\text{B-9})$$

applies, Eq (B-8) becomes

$$V_y^{(s)}(z) = -E_y^{\text{inc}}(h,0,z) d . \quad (\text{B-10})$$

Equations (B-4) and (B-5) show that

$$E_z^{(s)} = 0 \quad (\text{vertical polarization}) \quad (\text{B-11})$$

and

$$E_z^{(s)} = -ik \cos \psi \int_0^d E^{\text{inc}}(y,z) dy \quad (\text{horizontal polarization}). \quad (\text{B-12})$$

In our application the term $k_y d$ is taken as small compared to 1. The ~ 38 -ns rise time in Figure 5 suggests that frequencies up to ~ 26 MHz are important, with the main contributions to the pulse being at lower frequencies. Coupled with the $d = 14.5$ in. (36.8 cm) gives $k_{\text{max}} d < 0.2$. The exponent is further reduced (in our application at $\phi = -9.8^\circ$) by the factor $\sin 9.8^\circ = 0.17$. The restriction of (B-9) allows the horizontal-polarization term to be written as

$$E_z^{(s)} = -ik d \cos \psi E^{\text{inc}}(h,0,z) \quad (\text{horizontal polarization}). \quad (\text{B-13})$$

The case $\psi = 0$ is in agreement with Lee's Eq (41).^{B-4} Equation (B-10) is also consistent with Lee's data (allowing for coordinate differences). We seek a solution for Eqs (B-6) and (B-7) of the form

$$I(z) = [K_1 + P(z)] e^{ikz} + [K_2 + Q(z)] e^{-ikz} \quad (\text{B-14})$$

and

$$V(z) = V_y^{(s)}(z) + Z_0 \left\{ [K_1 + P(z)] e^{ikz} - [K_2 + Q(z)] e^{-ikz} \right\} . \quad (\text{B-15})$$

Direct substitution back into Eqs (B-6) and (B-7) yields

$$P(z) = 1/2Z_0 \int_{z_1}^z D^{(s)}(\zeta) e^{-ik\zeta} d\zeta$$

and

$$Q(z) = 1/2Z_0 \int_z^{z_2} D^{(s)}(\zeta) e^{ik\zeta} d\zeta,$$

where

$$D^{(s)}(z) = E_z^{(s)} - \partial V_y^{(s)}/\partial z$$

and

$$\partial V_y^{(s)}/\partial \zeta = ik \cos \psi \cos \phi V_y^{(s)}(\zeta).$$

Because of the $E_z^{(s)}$ variation in Eqs (B-11) and (B-13), the form for $D^{(s)}$ changes with the incident polarization.

$$D^{(s)}(z) = -ik d E^{\text{inc}}(h,0,z) A_1(\psi,\phi),$$

where

$$A_1(\psi,\phi) = \begin{cases} \cos \psi \cos \phi \sin \psi \sin \phi & \text{vertical polarization} \\ \cos \psi (1 + \cos^2 \phi) & \text{horizontal polarization.} \end{cases}$$

The constants K_1 and K_2 are determined from values of the terminating impedances Z_1 and Z_2 at the line positions $z = z_1$ and $z = z_2$ (where $z_2 > z_1$). To aid evaluation of these constants, we define the reflection coefficients as

$$\rho_1 = (Z_1 - Z_0)/(Z_1 + Z_0)$$

and

$$\rho_2 = (Z_2 - Z_0)/(Z_2 + Z_0).$$

When end 2 is open, $Z_2 = \infty$, and $\rho_2 = +1$. A short circuit at position 1 gives $Z_1 = 0$ and $\rho_1 = -1$. The impedance is given by $Z = \pm V/I$ for a wave traveling in the $+z$ (+) or $-z$ (-) direction. To arrive at z_1 , the wave traveling along the transmission line must be traveling in

the $-z$ direction. Thus we have $Z_1 = -V/I$ evaluated at $z = z_1$ and $Z_2 = +V/I$ evaluated at the other end. These two parameters fix the K_1 and K_2 as

$$K_1 = \frac{A(z_1) - \rho_1 Q(z_1) e^{-2ikz_1} - \rho_1 B(z_2) e^{-2ikz_1} + \rho_1 \rho_2 e^{2ikp} P(z_2)}{1 - \rho_1 \rho_2 e^{2ikp}},$$

$$K_2 = \frac{B(z_2) - \rho_2 P(z_2) e^{2ikz_2} - \rho_2 A(z_1) e^{2ikz_2} + \rho_1 \rho_2 e^{2ikp} Q(z_1)}{1 - \rho_1 \rho_2 e^{2ikp}},$$

where

$$A(z_1) = \frac{-V_y^{(s)}(z_1) e^{-ikz_1}}{Z_1 + Z_0},$$

and

$$B(z_2) = \frac{V_y^{(s)}(z_2) e^{ikz_2}}{Z_2 + Z_0}.$$

Appendix B References

- ¹American Institute of Physics Handbook, McGraw Hill, 1957, p 5-48.
- ²P. Naylor, C. Christopoulos, and P. B. Johns, *IEE Proceedings* 61:679(1987).
- ³C. D. Taylor, R. S. Satterwhite, and C. W. Harrison, Jr., *IEEE Trans Antennas and Propag* AP-13,987(1965).
- ⁴K. S. H. Lee, *IEEE Trans Electromag Compat* EMC-20,288(1978). The utility of a current-driver interpretation is discussed by K. S. H. Lee, *IEEE Trans Electromag Compat* EMC-23,44(1981).
- ⁵E. F. Vance, *Coupling to Shielded Cables*, Wiley, 1978. For a general discussion of EMP interactions, see K. S. H. Lee, Ed, *EMP Interaction: Principles, Techniques and Reference Data (A Handbook of Technology from the EMP Interaction Notes)*, Hemisphere Publishing Corporation, New York (distributed also by Springer-Verlag, Tokyo) 1986.

DISTRIBUTION:

- | | | | |
|---|---|---|--|
| 2 | Air Force Weapons Laboratory
Attn: NTAAB C. Baum
NTAT W. Page
Kirtland Air Force Base, NM 87117-6008 | 2 | Lawrence Livermore National Laboratory
Attn: L-84 H. Kruger
L-156 H. Cabayan
PO Box 808
Livermore, CA 94550 |
| 1 | Applied Physics Inc.
Attn: R. Knight
428 Louisiana Blvd. SE
Albuquerque, NM 87108 | 5 | Los Alamos National Laboratory
Attn: J. S. Malik/NSP/TO MS F670
R. Partridge
T. Young
M. Webb
M. Bernardin
PO Box 1663
Los Alamos, NM 87545 |
| 3 | Defense Nuclear Agency
Attn: RAEE
RAEV
APTL, Tech Library
6801 Telegraph Road
Alexandria, VA 22310-3398 | 3 | Metatech Corporation
Attn: W. A. Radasky
M. A. Messier
W. C. Hart
PO Box 1450
Goleta, CA 93116 |
| 1 | Electric Power Research Institute
Attn: M. Rabinowitz
Electrical Systems Division
3412 Hillview Avenue
Palo Alto, CA 94303 | 1 | Mission Research Corporation
Attn: C. L. Longmire
PO Drawer 719
Santa Barbara, CA 93102 |
| 1 | ElectroMagnetic Applications Inc.
Attn: D. E. Merewether
PO Box 8482
Albuquerque, NM 87198 | 1 | Oak Ridge National Laboratory
Attn: Randy Barnes
PO Box X
Oak Ridge, TN 37831 |
| 1 | Field Command Defense Nuclear Agency
Attn: FCTT W. Summa
Bldg 20363
Kirtland Air Force Base, NM 87115-5000 | 2 | Rand Corporation
Attn: C. Crain
W. Sollfrey
1700 Main Street
Santa Monica, CA 90406 |
| 2 | Harry Diamond Laboratories
Attn: DELHD-NW-EC W. T. Wyatt, Jr.
AMXDO-TI Tech Library
Department of the Army
2800 Powder Mill Road
Adelphi, MD 20783 | 1 | Research and Development Associates
Attn: R. L. Parker
2305 Renard Place SE
Albuquerque, NM 87119 |
| 1 | Kaman Sciences Corporation
Attn: Willard Hobbs
PO Box Drawer QQ
Santa Barbara, CA 93012 | 2 | Stanford Research Institute, International
Attn: A. L. Whitson
G. H. Price
333 Ravenswood Avenue
Menlo Park, CA 94025 |
| 1 | Kaman Tempo
DNA Information and Analysis Center
816 State Street
Santa Barbara, CA 93102 | | |

DISTRIBUTION (Continued):

1	Stanford Research Institute, International Attn: J. F. Prewitt 1900 Randolph Avenue SE Albuquerque, NM 87106	1	400	J. E. Gover
		1	1232	W. Beezhold
		1	1235	J. M. Hoffman
		1	1265	W. A. Johnson
		1	2300	J. L. Wirth
1	US Army Nuclear & Chemical Agency Attn: Adam F. Renner MONA-NU/Bldg 2073 Fort Belvoir, VA 22060-5858	1	2320	J. H. Renken
		1	2322	G. J. Scrivner
		1	2322	J. D. Kotulski
		1	2322	D. J. Riley
		1	2322	C. D. Turner
1	Westinghouse Electric Corporation Attn: C. H. Eichler 777 Penn Center Boulevard Pittsburgh, PA 15235	25	2322	C. N. Vittitoe
		1	2614	D. A. Rieb
		1	2813	N. I. Turner
		1	3151	E. R. Voelker
		1	3180	W. Van Deusen
3	Honolulu City-County Streetlight Dept Attn: Masao Bentosino 160 Koula Street Honolulu, HI 96813	1	6410	D. A. Dahlgren
		1	7523-1	A. J. Canute
		1	7553	M. E. Morris
		1	7553	K. C. Chen
1	West Virginia University Attn: Bernard R. Cooper Physics Department PO Box 6023 Morgantown, WV 26506-6023	1	7553	R. D. Jones
		1	7553	L. K. Warne
		1	7554	L. D. Scott
		1	7555	B. Boverie
		1	7555	S. W. Holmes
		1	9248	C. R. Mehl
3	Hawaiian Electric Company, Inc. Attn: Alan S. Lloyd PO Box 2750 Honolulu, HI 96840-0001	1	7555	G. A. Seely
		1	8524	J. A. Wackerly
		5	3141	S. A. Landenberger
		8	3141-1	C. L. Ward For DOE/OSTI
3	F. William Souza, Sr. 538 Kipuka Place Kailua District Oahu, HI 96734	3	3151	W. I. Klein
1	Louis F. Wouters Consultant, LLNL 321 Roxanne Drive Patterson, CA 95363			
1	Max Planck Institut fur Physik und Astrophysik Attn: John Mattox D-8046 Garching FEDERAL REPUBLIC OF GERMANY			